# PARAMETRIC ESTIMATION OF CLUTTER AUTOCORRELATION MATRIX FOR GROUND MOVING TARGET INDICATION

A THESIS SUBMITTED TO
THE GRADUATE SCHOOL OF NATURAL AND APPLIED SCIENCES
OF
MIDDLE EAST TECHNICAL UNIVERSITY

BY

EMRE KALENDER

IN PARTIAL FULFILLMENT OF THE REQUIREMENTS
FOR
THE DEGREE OF MASTER OF SCIENCE
IN
ELECTRICAL AND ELECTRONICS ENGINEERING

JANUARY 2013

Approval of the thesis:

**PARAMETRIC ESTIMATION OF CLUTTER AUTOCORRELATION MATRIX FOR GROUND MOVING TARGET INDICATION**

submitted by **EMRE KALENDER** in partial fulfillment of the requirements for the degree of **Master of Science in Electrical and Electronics Engineering Department, Middle East Technical University** by,

Prof. Dr. Canan Özgen _____
Dean, Graduate School of **Natural and Applied Sciences**

Prof. Dr. İsmet Erkmen _____
Head of Department, **Electrical and Electronics Engineering**

Prof. Dr. Yalçın Tanık _____
Supervisor, **Electrical and Electronics Eng. Dept., METU**

**Examining Committee Members:**

Prof. Dr. Mete Severcan _____
Electrical and Electronics Engineering Dept., METU

Prof. Dr. Yalçın Tanık _____
Electrical and Electronics Engineering Dept., METU

Assoc. Prof. Dr. Ali Özgür Yılmaz _____
Electrical and Electronics Engineering Dept., METU

Assoc. Prof. Dr. Çağatay Candan _____
Electrical and Electronics Engineering Dept., METU

Dr. Ülkü Çilek Doyuran _____
Radar System Engineering Division, ASELSAN

**Date:** _____

**I hereby declare that all information in this document has been obtained and presented in accordance with academic rules and ethical conduct. I also declare that, as required by these rules and conduct, I have fully cited and referenced all material and results that are not original to this work.**

Name, Last Name: EMRE KALENDER

Signature :

# ABSTRACT

PARAMETRIC ESTIMATION OF CLUTTER AUTOCORRELATION MATRIX FOR GROUND MOVING TARGET INDICATION

Kalender, Emre

M.S., Department of Electrical and Electronics Engineering

Supervisor : Prof. Dr. Yalçın Tanık

January 2013, 68 pages

In airborne radar systems with Ground Moving Target Indication (GMTI) mode, it is desired to detect the presence of targets in the interference consisting of noise, ground clutter, and jamming signals. These interference components usually mask the target return signal, such that the detection requires suppression of the interference signals. Space-time adaptive processing is a widely used interference suppression technique which uses temporal and spatial information to eliminate the effects of clutter and jamming and enables the detection of moving targets with small radial velocity. However, adaptive estimation of the interference requires high computation capacity as well as large secondary sample data support. The available secondary range cells may be fewer than required due to non-homogeneity problems and computational capacity of the radar system may not be sufficient for the computations required. In order to reduce the computational load and the required number of secondary data for estimation, parametric methods use a priori information on the structure of the clutter covariance matrix. Space Time Auto-regressive (STAR) filtering, which is a parametric adaptive method, and full parametric model-based approaches for interference suppression are proposed as alternatives to STAP in the literature. In this work, space time auto-regressive filtering and model-based GMTI approaches are investigated. Performance of these approaches are evaluated by both simulated and flight test data and compared with the performance of sample matrix inversion space time adaptive processing.

Keywords: GMTI, Parametric, Suppression, Clutter, Auto-regressive

# ÖZ

HAREKETLİ YER HEDEFİ TESPİTİ UYGULAMALARINDA KARGAŞA ÖZİLİNTİ MATRİSİNİN PARAMETRİK KESTİRİMİ

Kalender, Emre

Yüksek Lisans, Elektrik Elektronik Mühendisliği Bölümü

Tez Yöneticisi : Prof. Dr. Yalçın Tanık

Ocak 2013, 68 sayfa

Hareketli yer hedefi tespiti (GMTI) modu olan hava radar sistemlerinde kargaşa, karıştırıcılar ve gürültü sinyalleri içinde bulunan hareketleri hedeflerin tespiti istenmektedir. Bu girişim bileşenlerinin genellikle hedef yankı sinyallerini maskelemesi nedeniyle girişim sinyallerinin bastırılması gerekmektedir. Uzay zaman uyarlı işleme, uzaysal ve zamana bağlı bilgileri kullanan ve yaygın biçimde kullanılan bir girişim bastırma tekniğidir ve düşük radyal hızlara sahip hedeflerin tespitini mümkün kılmaktadır. Ancak, girişimin uyarlamalı bir biçimde kes- tirimi geniş ikincil veri desteği yanında yüksek işlem kapasitesi gerektirmektedir. Homojen olmama problemleri nedeniyle ikincil veri desteği gerekenden az olabilmektedir ve radar sisteminin işlem kapasitesi uyarlamalı kestirim için yeterli olamayabilmektedir. İşlem yükünü ve kestirim için gerekli olan ikincil veri gereksinimini azaltabilmek amacıyla parametrik metodlar kargaşa ilinti matrisinin yapısına ilişkin önceden sahip olunan bilgileri kullanmaktadır. Girişim bastırımı için parametrik uyarlamalı bir yöntem olan uzay zaman özbağlanımlı filtreleme ve tam parametrik bir yöntem olan model bazlı metodlar, uzay zaman uyarlı işlemeye alternatif olarak literatürde önerilmiştir. Bu çalışmada, uzay zaman özbağlanımlı filtreleme ve model bazlı GMTI yaklaşımları incelenmiştir. Bu yaklaşımların performansları hem benzetim hem de test uçuşu verileri ile değerlendirilmiş ve örnek matris çevrimi uzay zaman uyarlı işleme ile performans karşılaştırılması yapılmıştır.

Anahtar Kelimeler: GMTI, Parametrik, Bastırım, Kargaşa, Özbağlanımlı

*To My Family*

# ACKNOWLEDGMENTS

This thesis was written with the help and assistance of various people and I would like to take this opportunity to acknowledge the tremendous help they have given me while I was completing my thesis.

Firstly, I would like to thank Prof. Dr. Yalçın Tanık, for his counselling, technical help and guidance which help me stay always in the right direction.

Secondly, I would like to thank Çağdaş Kocabıyık and Ozan Bilgin for their assistance in my personal life which enabled me to focus on my thesis work.

I would like to thank my lovely parents for their help, support and trust they have given me all along my life.

I would address my finally thanks to ASELSAN.

This thesis was supported by TÜBİTAK Scholarship for MS Students.

# TABLE OF CONTENTS

# LIST OF TABLES

TABLES

# LIST OF FIGURES

FIGURES

# LIST OF ABBREVIATIONS

ABBREVIATIONS

GMTI – Ground Moving Target Indication
STAP – Space Time Adaptive Processing
ICM – Internal Clutter Motion
LDU – Lower Diagonal Unitary
STAR – Space Time Auto-Regressive Filtering
DL-SMI – Diagonally Loaded Sample Matrix Inversion
METU – Middle East Technical University
EEE – Electrical Electronical Engineering
PAMF – Parametric Adaptive Matched Filtering
NHD – Non-Homogeneity Detector
CFAR – Constant False Alarm Rate
MDV – Minimum Detectable Velocity
AIC – Akaike Information Theoretic Criterion
MDL – Minimum Description Length
SAR – Synthetic Aperture Radar
RCS – Radar Cross Section
SINR – Signal to Interference plus Noise Ratio
AR – Auto-Regressive
DPCA – Displaced Phase Center Antenna
ATI –Along Track Interferometry
SCR – Signal to Clutter Ratio
ULA –Uniform Linear Array
CPI – Coherent Processing Interval
MR –Mean Ratio
VI – Variability Index
IP-NHD –Inner Product Non-Homogeneity Detector
DTED – Digital Terrain Elevation Data

# CHAPTER 1

# INTRODUCTION

## 1.1 Thesis Motivation and Objective

In airborne radar systems with GMTI mode, it is desired to detect the presence of targets in the interference consisting of noise, ground clutter, and jamming signals if a jammer is present. These interference components usually mask the target return signal, such that the detection requires suppression of the interference signals. Space-time adaptive processing (STAP) is a widely used interference suppression technique in airborne radar systems. STAP methods use temporal and spatial information jointly to eliminate the effects of clutter and jamming. The main advantage of STAP methods is the detection of moving targets that are close to the interference subspace due their small radial velocity. However, adaptive estimation of the interference exposes heavy computational load in the implementation and heavily depend on the number of secondary range bins used in the interference estimation process. The available secondary range cells may be fewer than required due to non-homogeneity problems and it is known that computational load of such algorithms are crucial for system processor design.

In order to reduce the computational load and the required number of secondary range bins for estimation, structure-based and model-based approaches for interference suppression have been proposed in the literature. Unlike STAP methods, these methods do not assume that the interference is completely unknown. The aim of this work is to make use of the a priori knowledge of the interference structure through structure-based and model-based methods to achieve interference suppression with reduced computational load and secondary range bins.

Previous studies conducted on this subject include

- Usage of multichannel auto-regressive filter for interference characterization such as Parametric Adaptive Matched Filtering (PAMF) [8] and Space Time Auto-regressive Filtering (STAR) [10, 11].
- Usage of a interference covariance matrix model for clutter suppression [25].

The work done in this thesis aims to

- Implement Space Time Auto-regressive Filtering and present results obtained with the implementation of the proposed approach in the literature.
- Form an interference covariance matrix model and present results obtained with the model-based approach that uses the proposed model.

The work done in this thesis additionally aims to perform the following operations

- Auto-regressive filter order determination.
- Clutter power estimation under non-homogenous clutter enviroment.

The mentioned structure based and model based approaches are implemented and applied to simulated GMTI data and GMTI data acquired during flight trials with the experimental SAR system. The results indicate that

- Suppression of interference with fewer secondary range bins can be achieved by STAR filtering.
- Interference suppression is possible by model-based clutter suppression.

## 1.2 Literature Survey

Radars are widely used for collecting fast and accurate warfare intelligence for national border protection. Movements of objects (vehicles, man) in an area of interest are generally the most tactically crucial information. Airborne platforms are resourceful for such information gathering due to their mobility. However, detection of slow moving ground targets is a very challenging problem, since the stationary ground clutter points have relative velocity with respect to the airborne platform as a result of the radar platform velocity. The relative motion between the radar and the clutter creates a Doppler bandwidth in the Doppler spectrum. Targets that fall in this Doppler spectrum have low signal-to-interference ratio (SIR) which results in a reduced detection performance. Such targets are called endoclutter targets.

Space–time adaptive processing (STAP) is a widely used technique for improving signal-to-interference ratio of endoclutter targets [1, 2, 3]. STAP adaptively forms two dimensional (Space and Time) filters according to the interference environment in an attempt to maximize the output SIR. Efficient filtering for interference suppression is performed using adaptive filters on observation data collected by $M$ antenna elements over $N$ pulses in a coherent processing interval (CPI). For fully adaptive STAP, the most important step is the estimation of the $MN$–variate interference covariance matrix, which requires the number of independent identically distributed (i.i.d.) secondary data samples to be larger than $2MN$ to guarantee that the average SIR loss is no more than, say 3 dB, with respect to the SIR that could be obtained when the actual interference covariance matrix is known[4]. However, adaptive estimation of the interference exposes heavy computational load on the processors and it heavily depends on the number of secondary range bins used in the interference estimation process. The available secondary range cells may be fewer than what is required due to non-homogeneity problems and it is known that computational load of STAP algorithms are the bottleneck for system processor design. To solve these problems, reduced-rank STAP techniques have been proposed in the literature, such as the principal components inverse algorithm [5] and loaded sample matrix inversion (LMSI) method [6] . These techniques can operate with fewer secondary range bins to a number on the order of twice the number of dominant eigenvectors of the interference covariance matrix [7].

However, in practice the available computation power and secondary range bins can be fewer than required for the reduced rank STAP methods. Under these circumstances, structure-based and model-based approaches can be considered as an alternative. Structure-based approaches are adaptations of STAP algorithms that are based on the use of multi-channel autoregressive (AR) models, while model-based approaches use clutter covariance matrix models based on the platform and radar parameters in order to construct the interference covariance matrix estimation.

In [8], parametric adaptive matched filtering (PAMF) for STAP and detection is presented. The PAMF approach is based on estimating the interference structure with a low order multichannel autoregressive model. Since the model order of the autoregressive model is low, dominant eigenvalues of the estimated covariance matrix for PAMF is fewer than that for the full-rank STAP. Therefore fewer secondary data are required for estimation. LDU decomposition of the interference covariance

matrix is also presented in [8]. Least squares method is suggested for filter coefficient determination. The spatial and temporal whitening are both performed by a two stage whitening process since the estimation of the PAMF filter coefficients are achieved by not only averaging measures in the fast time (range direction) but also in the slow-time direction. In [9], PAMF filter coefficients are derived by employing the least squares method.

In [11], Space-Time Auto-Regressive (STAR) filtering is presented. STAR filtering, which is a parametric matched subspace detector, uses an AR vector model to estimate the orthogonal subspace to interference signals. Once this subspace is found, it is used to suppress the interference signal before detection. Similar to PAMF, least squares method is proposed for filter coefficient determination. Solution by the least squares method converges to the singular value decomposition of a matrix composed of secondary data inputs. Three specific implementations of the STAR filter for detection have been proposed: Auto-Regressive Filtered Generalized Likelihood Ratio test (ARGLRT), Diagonally Loaded STAR (STARDL) test, and the STAR Prediction Error tests. The performance of these techniques are evaluated. The STAR Prediction Error test does not require inverse of a matrix and its performance is very near to other tests. Therefore, in the scope of this thesis the STAR methods are preferred using STAR Prediction Error test. In [10], the STAR filter order estimation is accomplished by adaptations of Akaike information theoretic criterion (AIC) [13] and the minimum description length (MDL) criterion [12]. Filter order estimators are tested with simulated data for different scenarios.

A clutter covariance matrix model for side-looking GMTI geometry was modeled by Yalçın Tanık [25]. The model is built on the assumptions that the area illuminated by the antenna beam is flat, each clutter scatterer point is statistically independent, inter-clutter motion is not present, the distance traveled during a coherent processing interval is much less than the range and maximum distance between receive antenna phase centers is much less than the range. In this model, the only parameter to be estimated is the mean clutter radar cross section. In this model, due to the inhomogeneities of the clutter along the range direction arising with discrete clutter or clutter edges, clutter power may be overestimated or underestimated. In order to deal with these inhomogeneities non-homogeneity detectors or intelligent power estimation methods can be used. In [14], impact of secondary data selection on the STAP performance is illustrated. A non-homogeneity detection scheme to improve secondary data selection is suggested. The nonhomogeneity detectors discussed are the inner product, generalized inner product and the sample matrix inversion test statistic methods. These three methods are evaluated by measured airborne data. Non-homogeneity detection is performed by considering each secondary data individually and detecting the outliers by setting a threshold on the variance of the detector output and by using a two hypothesis test for homogeneity and non-homogeneity. After the removal of the outliers, estimation is repeated for remaining secondary data. In [15], an intelligent CFAR (constant false alarm rate) was proposed. Intelligent CFAR is a technique that switches to the techniques SO-CFAR (smallest of CFAR), GO-CFAR (greates of CFAR) or CA-CFAR (cell averaging CFAR) depending on the characteristics of the interference in the secondary data. Secondary data is divided into two groups, leading and lagging windows. By investigating each window, variability and mean ratio index values are obtained. Variability index is a measure for determining the inhomogeneities by using the variance of the secondary data in in the window under test, while mean ratio test is used for detecting the clutter edges that occur between the leading and lagging windows. Using the mentioned index values the intelligent CFAR chooses the most suitable CFAR method among SO-CFAR, GO-CFAR or CA-CFAR.

## 1.3 Previous Related Work in METU EEE Department

This thesis is a part of the Ground Moving Target Indication research field. The following theses ,that are published in the past and related to the Ground Moving Target Indication research area, have been resourceful during the development of this thesis.

- "Simulation Based Comparison of Some GMTI Techniques" [17] : The work done in this thesis aims to compare the detection performances of several GMTI techniques such as DPCA, ATI

and STAP by means of using simulated radar data.

- "Antenna Patterns for Detecting Slowly Moving Targets in Two Channel GMTI Processing" [18]: This thesis focuses on obtaining optimal antenna patterns for a two channel radar sensor in an attempt to optimize detection performance of endoclutter targets.

- "Interference Suppression by Using Space Time Adaptive Processing for Adaptive Radar" [19]: This thesis establishes the space-time signal model and uses simulated data in order to compare the detection performances of the DPCA and the Optimal STAP techniques.

- "A Knowledge Based Approach in GMTI for The Estimation of the Clutter Covariance Matrix in Space Time Adaptive Processing" [20]: This thesis proposes a knowledge based approach which makes use of both a priori and instantaneous data for the clutter covariance matrix estimation process. The approach proposed is implemented and applied to the GMTI data acquired during flight trials with the experimental SAR system.

## 1.4 Thesis Outline

Chapter 2 details the background information needed to understand the GMTI concept and interference suppression problem as well as the PAMF and Sample Matrix Inversion Pre-Doppler STAP. Chapter 3 covers STAR filtering details. Chapter 4 introduces a model for clutter covariance matrix and clutter power estimation including inner product non-homogeneity detector and intelligent clutter power estimation methods. Chapter 5 presents the simulation technique used and the simulation results for each suppression technique explained in Chapter 3 and Chapter 4. This chapter also includes the flight test results. Finally, conclusions are presented in Chapter 6 and possible future work is discussed for prospective enhancements.

# CHAPTER 2

# BACKGROUND

## 2.1 GMTI Geometry

In the GMTI surveillance which is an air-to-ground mode, geometry is defined by both the platform flight parameters and radar data acquisition parameters. These parameters define the position of the radar antenna phase center and extent and the area being observed.

The platform altitude and platform velocity are two basic properties of the GMTI geometry which are defined by the platform flight parameters. The characteristics of the GMTI geo- metry are mainly determined by the radar data acquisition parameters. In Figure 2.1, a side view of the GMTI geometry is depicted. Point T is the location of the target. Point N is the nadir point of the radar antenna which is the projection of the radar antenna phase center on the ground. Point P is the actual position of the radar antenna phase center. The ground range $r'$, is the distance between the nadir point and the target which is illustrated by the line connecting points N and T. The distance between the antenna phase center and the target is called the slant range $r$ which is illustrated by the line connecting points P and T. In this thesis, the term range is used for describing the slant range. Another important parameter is the grazing angle $\beta$. Grazing angle is defined as the angle between the range line and ground plane.

GMTI mode is a side-looking mode. The observation area may be located at either left or right side of the platform flight direction and the radar line of sight is perpendicular to the flight direction. However, operational needs may require that radar line of sight not to be perpendicular to the platform flight direction. In Figure 2.2, top view of the GMTI geometry can be observed. Point L is the intersection of the ground and radar line of sight. Point P is the actual position of the radar antenna phase center. Platform velocity vector is shown with vector $\vec{V}$. Radar line of sight is the vector connecting the points

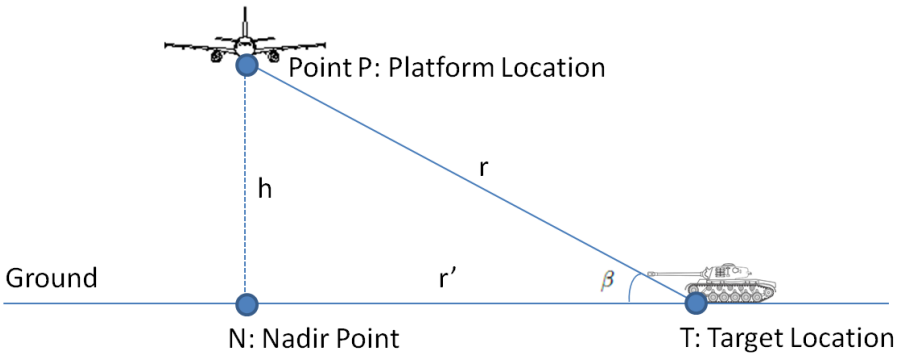


Figure 2.1: Side View of the GMTI Geometry

P and L. The angle between the platform velocity vector and the radar line of sight is called the squint angle $\phi$.

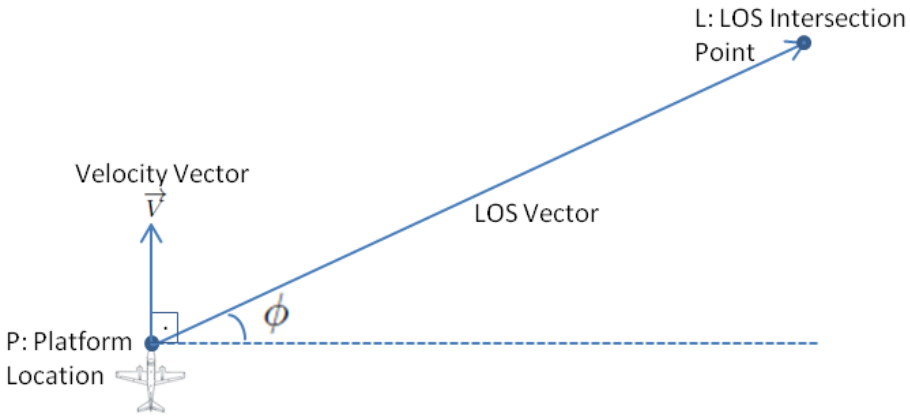


Figure 2.2: Top View of the GMTI Geometry

Since the grazing angle is greater than zero, the slant range resolution $\Delta r$ and the ground range resolution $\Delta r'$ are different. The slant range resolution is defined as resolution on the slant plane. Slant range resolution for a pulsed GMTI radar can be found as

$$\Delta r = \frac{c\tau}{2} \tag{2.1}$$

where $\tau$ is the pulse width of the radar and $c$ is the velocity of light. However it should be noted that linear frequency modulated waveforms are commonly used for GMTI radars. In such a case the slant range resolution is

$$\Delta r = \frac{c}{2B_{radar}} \tag{2.2}$$

where $B_{radar}$ is the bandwidth of the transmitted pulse.

The projection of the slant range resolution on ground is called the ground range resolution and can be found as

$$\Delta r' = \frac{\Delta r}{\cos\beta}. \tag{2.3}$$

The distance between two points at range $r$ for an azimuth beamwidth of $\theta_{3,az}$ is called as the cross-range resolution $\Delta r_{cross}$.

$$\Delta r_{cross} = r\theta_{3,az}. \tag{2.4}$$

The grazing angle, antenna azimuth beamwidth $\theta_{3,az}$ and range resolution parameters define the iso-range lines on the ground , which are the collection of points that are in the same range bin. The isorange line area $A_{iso}$ can be found as:

$$A_{iso} = \Delta r_{cross}\Delta r' = \frac{r\theta_{3,az}\Delta r}{\cos\beta}. \tag{2.5}$$

GMTI modes aim to detect targets moving on ground which are in strong clutter areas. Large iso-range line areas form larger echo clutter powers at the radar receiver. Therefore, the minimization of the iso-range line area and maximization of the Signal-to-Clutter Ratio (SCR) are crucial for the detection of slow moving ground targets.

Another radar parameter to be set for GMTI radars is the Pulse Repetition Frequency (PRF). For unambiguous operation, both in range and Doppler, PRF must be chosen considering the maximum

unambiguous range $r_{unamb}$ whose relationship with PRF is given below:

$$r_{unamb} = \frac{c\,PRF}{2}. \tag{2.6}$$

The distance traveled between two consecutive pulses $\Delta x$ can be expressed as

$$\Delta x = \frac{v}{PRF} \tag{2.7}$$

where $v$ is the platform velocity. The correlations of the clutter echoes between pulses in a coherent integration interval are heavily dependent on $\Delta x$. The relationship of the clutter correlations with radar and platform parameters will be explained in section 4.1.

## 2.2 Doppler in GMTI

For a radar mounted on a moving platform, platform motion spreads the ground clutter signal to the clutter Doppler spectrum. It is known that the Doppler shift for a radar with a platform moving with velocity $v$ with its antenna boresight squinted $\phi$ radians with respect to the platform velocity vector is

$$F_D = \frac{2v}{\lambda}\cos(\phi) \tag{2.8}$$

where the radar wavelength is $\lambda$.

Let the most squinted point of the clutter in 3 dB beamwidth of the radar antenna be P1 and the least squinted point of the clutter in 3 dB beamwidth of the radar antenna be P2 as shown in Figure 2.3.

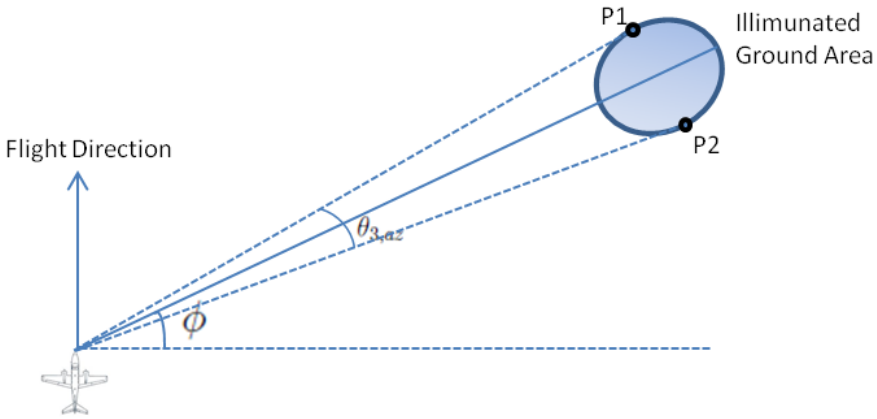


Figure 2.3: Radar Illumination Area and Related Doppler Spreads

Doppler shifts corresponding to the 3 dB beamwidth edges P1 and P2 can be expressed as [17]

$$F_{D,max} = \frac{2v}{\lambda}\cos\left(\phi + \frac{\theta_{3,az}}{2}\right), \tag{2.9}$$

$$F_{D,min} = \frac{2v}{\lambda}\cos\left(\phi - \frac{\theta_{3,az}}{2}\right) \tag{2.10}$$

where the azimuth 3 dB beamwidth of the antenna is $\theta_{3,az}$. Then the clutter Doppler spread $\beta_D$ is

$$\beta_D = F_{D,max} - F_{D,min}. \tag{2.11}$$

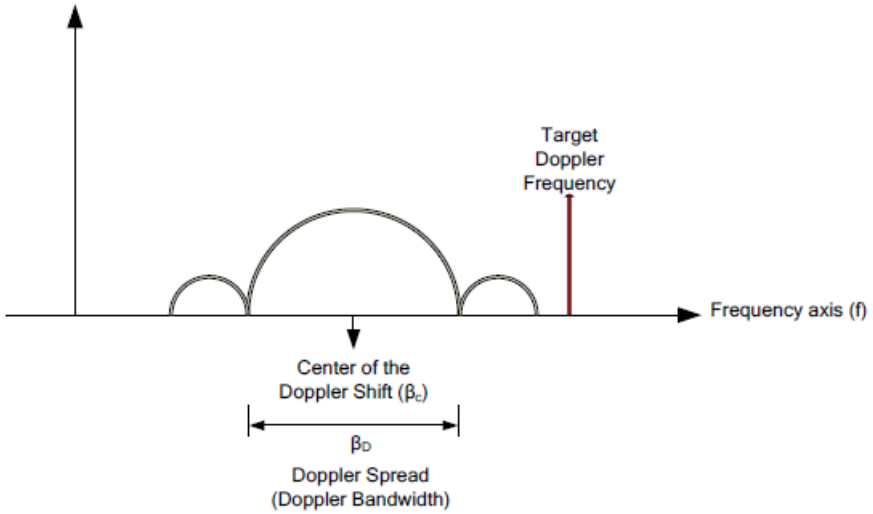


Figure 2.4: Doppler Spectrum for Exoclutter GMTI[17]

Doppler bins that corresponds to the Doppler frequencies outside of the frequency band between $F_{D,max}$ and $F_{D,min}$ are called the exoclutter region. Figure 2.4 demonstrates a target present in the exoclutter region.

Doppler bins that corresponds to the Doppler frequencies between $F_{D,max}$ and $F_{D,min}$ are called the endoclutter region. Figure 2.5 demonstrates a target present in the endoclutter region. The minimum detectable velocity is often determined by the endoclutter region.

## 2.3 Minimum Detectable Velocity

GMTI modes of the radar are used for the remote detection of non-stationary ground objects. GMTI data are obtained from range-slow time maps of the illuminated area, in which radar cross section (RCS) is measured as a function of range and slow time. Maps that contain the radial velocity with respect to the radar platform of the targets that are in the illuminated area, can be derived from the data acquired. These maps will be called as range-Doppler maps. All GMTI modes are characterized by a minimum detectable radial velocity (MDV). Targets that have a smaller radial velocity than MDV, can not be distinguished from ground clutter which has the same relative motion with respect to the platform. If these targets have small RCS, then they are most likely overwhelmed by ground clutter returns, and therefore they are usually not detectable.

The MDV of a GMTI radar is determined by the various parameters, including[21]:

- Platform velocity $v$
- Platform altitude $h$, relative to the ground at scene center
- Antenna azimuth beamwidth $\theta_{3,az}$
- Grazing angle $\theta$
- Imaging squint angle $\phi$

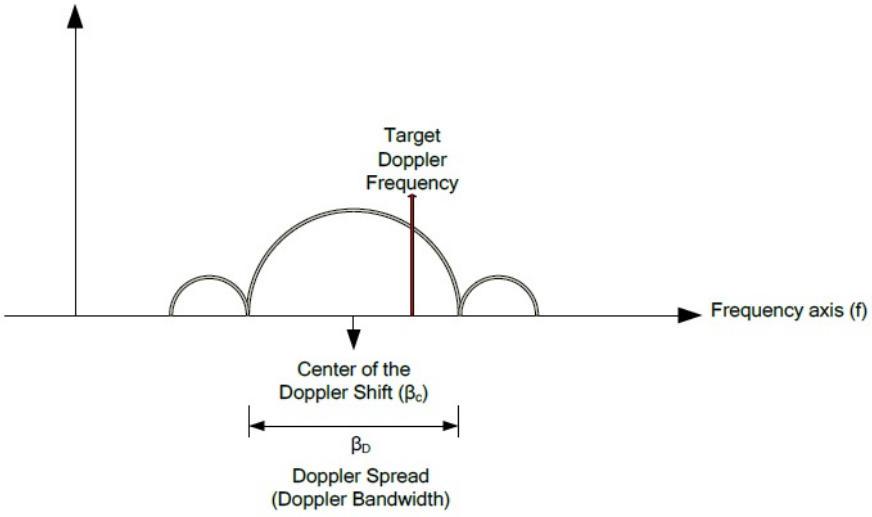


Figure 2.5: Doppler Spectrum for Endoclutter GMTI[17]

• Ground range resolution $\Delta r'$

These parameters impact MDV because they dictate the extent of the imaged scene on the ground and the relative motion of different ground points across that extent. The collective set of all imaged ground points comprises the endoclutter region bandwidth and the clutter power for an iso-range line. For small MDV values, high SCR values are mandatory and high SCR for endo-clutter clutter regions can be obtained via clutter suppression techniques.

## 2.4 Optimum Detector

A radar system with M active antennas and N pulses in a coherent processing interval (CPI) is assumed. The data sampled for the $n$th pulse at the $m$th antenna output will be denoted as $z_{n,m}$. The acquired data vector $\mathbf{z}$, which is of size $MN$ x 1, is defined as

$$\mathbf{z} = \begin{bmatrix} \mathbf{z}(1) \\ \mathbf{z}(2) \\ \vdots \\ \mathbf{z}(N-1) \\ \mathbf{z}(N) \end{bmatrix} \tag{2.12}$$

where $\mathbf{z}(n)$ are vectors of size $M$ x 1 and defined as

$$\mathbf{z}(n) = \begin{bmatrix} z_{n,1} \\ z_{n,2} \\ \vdots \\ z_{n,(m-1)} \\ z_{n,m} \end{bmatrix}. \tag{2.13}$$

The data vector can be expressed under different hypotheses for target presence and absence as follows

$$H_0 \rightarrow \mathbf{z} = \mathbf{c} + \mathbf{j} + \mathbf{n} \tag{2.14}$$

$$H_1 \rightarrow \mathbf{z} = \mathbf{c} + \mathbf{j} + \mathbf{n} + \mathbf{b}s \tag{2.15}$$

where **c**: clutter signal **j**: jammer signal (if present) **n**: thermal noise signal (zero mean White Gaussian) $s$: target radar cross section model ( Swerling-I assumption) **b**: space time target steering vector which are all vectors of size $MN$ x 1.

The covariance matrix of **z** under different hypotheses can be denoted as

$$H_0 \rightarrow R_0 = R_c + R_j + \sigma_n^2 I \tag{2.16}$$

$$H_1 \rightarrow R_1 = R_0 + \sigma_s^2 bb^h \tag{2.17}$$

where $I$ is the identity matrix of size $MN$ x $MN$, $\sigma_n^2$ is the thermal noise power and $\sigma_s^2$ is the target power.

The optimum detector used for a zero mean Gaussian detection problem can be expressed as [2]

$$l = \mathbf{z}^H Q \mathbf{z} \underset{H_1}{\overset{H_0}{\lessgtr}} \gamma \tag{2.18}$$

where $\gamma$ is the detection threshold and $Q$ is a matrix of size $MN$ x $MN$ as

$$Q = R_0^{-1} - R_1^{-1}. \tag{2.19}$$

However, $R_0$ is usually unknown. Therefore, the covariance matrix of the interference $R_0$ should be estimated using supporting data or from a model of the covariance matrix.

## 2.5 Matched Filter Detector

Matched filtering is a commonly used sub-optimum method that aims to maximize the signal-to-interference ratio (SINR) at the output of the filter. The matched filter coefficients can be expressed as[2]

$$\mathbf{w}_{MF} = \gamma R_u^{-1} \mathbf{b} \tag{2.20}$$

where $R_u$ is the interference covariance matrix which is the covariance under no target hypo- thesis, $\gamma$ is a complex constant and $\boldsymbol{b}$ is the space-time target steering vector that corresponds to the target whose presence is being tested in the test data.

For the sake of simplicity $\gamma$ will be assumed to be unity. The matched filter output $\boldsymbol{y}$ can be expressed as

$$\mathbf{y} = \mathbf{w}_{MF}^H \mathbf{z} \tag{2.21}$$

where **z** is the data vector under test.

Improvement provided by the matched filter increases as the input signal characteristics differ more from the interference characteristics. The signal-to-interference ratio at the output of the matched filter can be found as

$$SINR_{MF} = \frac{E\{(\mathbf{w}_{MF}^H \mathbf{bs})^H (\mathbf{w}_{MF}^H \mathbf{bs})\}}{E\{(\mathbf{w}_{MF}^H \mathbf{z}_u)^H (\mathbf{w}_{MF}^H \mathbf{z}_u)\}} = \sigma_s^2 \mathbf{b}^H R_u^{-1} \mathbf{b}. \tag{2.22}$$

Power of the weighting vector response to the target space time steering vector is called adapted pattern and expressed as

$$P_{MF} = \mid \mathbf{w}_{MF}^H \mathbf{b} \mid^2 . \tag{2.23}$$

For a signal amplitude that is unknown, the detection test statistic used in the matched filter processing is the power ratio of the output projection on target steering vector power to the power of interference and noise projection on target steering vector.[3]

$$l_{MF} = \frac{|\mathbf{w}_{MF}^H \mathbf{z}|^2}{\left|\mathbf{w}_{MF}^H \mathbf{b}\right|} = \frac{|\mathbf{b}^H R_u^{-1} \mathbf{z}|^2}{\left|\mathbf{b}^H R_u^{-1} \mathbf{b}\right|}. \tag{2.24}$$

## 2.6 Sample Matrix Inversion Pre-Doppler Space Time Adaptive Processing Approach

### 2.6.1 Interference Covariance Matrix Estimation

Adaptive interference covariance estimation is a technique that uses the neighbor range bin data in order to estimate the interference covariance in the range bin under test. The data vectors corresponding to the mentioned range bins are called secondary data and will be shown as $\mathbf{z}_k$. If $K$ secondary data vectors are used the estimate the interference covariance matrix $R_u$, then the estimator is [5]

$$\hat{R}_u = \frac{1}{K} \sum_{k=1}^{K} \mathbf{z}_k \mathbf{z}_k^H. \tag{2.25}$$

It should be noted that the estimator assumptions are that the secondary range bins are target free and the interference is homogenous for the secondary range bins. The estimator described in (2.25) is called the Sample Matrix Inversion (SMI) estimator. A method that is generally used is the diagonally-loaded sample matrix (DL-SM) method that uses an identity matrix load with a magnitude comparable with thermal noise power. [5]

$$\hat{R}_u = \delta I + \frac{1}{K} \sum_{k=1}^{K} \mathbf{z}_k \mathbf{z}_k^H \tag{2.26}$$

where $\delta$ is a constant of the system thermal noise level order and $I$ is the identity matrix.

### 2.6.2 SMI Pre-Doppler STAP Weighting Vector

The matched filter coefficients can be expressed as [22]

$$W_{AMF} = \hat{R}_u^{-1} \mathbf{b} \tag{2.27}$$

where $\mathbf{b}$ is the space-time target steering vector. Then the final form of the detection test statistics is

$$l_{AMF} = \frac{\left|\mathbf{b}^H \hat{R}_u^{-H} \mathbf{z}\right|^2}{\mathbf{b}^H \hat{R}_u^{-H} \mathbf{b}}. \tag{2.28}$$

The weight vector requires $O((MN)^3 + (MN)^2)$ flops to compute since calculation of the inverse of a matrix of size $A$ x $B$ matrix requires $O((AB)^3)$ flops . To find the estimated clutter covariance matrix, $O((MN)^2 K)$ flops are required. The computational complexity can be estimated as

$$AMF_{flop} = O((MN)^3 + (MN)^2) + O((MN)^2 K)). \tag{2.29}$$

The signal to inference ratio at the output of the filter is

$$SINR_{AMF} = \frac{\sigma_s^2 \left|\mathbf{b}^H \hat{R}_u^{-H} \mathbf{b}\right|^2}{\mathbf{b}^H \hat{R}_u^{-H} R_u \hat{R}_u^{-1} \mathbf{b}}. \tag{2.30}$$

To achieve a good performance with this detector, a reasonable estimate $\hat{R}_u$ is required, which in turn requires $K$ secondary range bins which is at least larger than the clutter rank. The clutter rank is often described by the Brennan's rule for uniform linear array antennas (ULA). For circular array antennas the rank of the clutter can be estimated as double of the rank calculated for the ULA case. The clutter rank $\rho$ for ULA can be expressed as [23]

$$\rho = M + (N-1)\beta \tag{2.31}$$

where $\beta$ is

$$\beta = \frac{2v}{f_{prf}d} \tag{2.32}$$

where $d$ is the distance between the antennas, $f_{prf}$ is the pulse repetition frequency and $v$ is the platform velocity. $\beta$ usually takes values between 0.5 to 1.5. In these cases the required secondary data is large and often not available due to clutter inhomogeneity. For circular arc arrays, clutter rank can be estimated roughly twice of the predicted by Brennan's rule [24]. SMI Pre-Doppler STAP approach is to be used for comparison purposes throughout this thesis.

## 2.7 Parametric Adaptive Matched Filtering Approach

### 2.7.1 LDU Decomposition of Interference Covariance Matrix

Any positive definite and Hermitian matrix has an LDU decomposition which can be shown as

$$C = ABA^H \tag{2.33}$$

where $A$ is a lower-block triangular matrix and $B$ is a diagonal matrix.

In order to express the matched filter detection test statistics in a different way, the LDU decomposition of interference covariance matrix $R_u$will be investigated. The LDU decomposition of the interference covariance matrix can be expressed as [8]

$$R_u = ADA^H \tag{2.34}$$

where $A$ is a lower-block triangular matrix and $D$ is diagonal matrix. Then the inverse of $R_u$ can be expressed as

$$R_u^{-1} = A^{-H}D^{-1}A^{-1} = A^{-H}D^{-1/2}D^{-1/2}A^{-1}. \tag{2.35}$$

Note that since $D$ is a diagonal matrix, its inverse $D^{-1}$is also diagonal as well as $D^{-1/2}$.

Then the detection test statistics can be shown as [13]

$$l_{MF} = \frac{|\mathbf{b}^H R_u^{-H}\mathbf{z}|^2}{\left|\mathbf{b}^H R_u^{-H}\mathbf{b}\right|} = \frac{|\mathbf{b}^H A^{-H}D^{-1/2}D^{-1/2}A^{-1}\mathbf{z}|^2}{\left|\mathbf{b}^H A^{-H}D^{-1/2}D^{-1/2}A^{-1}\mathbf{b}\right|}, \tag{2.36}$$

$$l_{MF} = \frac{|(D^{-1/2}A^{-1}b)^H(D^{-1/2}A^{-1}\mathbf{z})|^2}{(D^{-1/2}A^{-1}b)^H(D^{-1/2}A^{-1}b)}. \tag{2.37}$$

The vectors $\mathbf{u}$ and $\epsilon$ are defined as

$$\mathbf{u} = A^{-1}\mathbf{b}, \tag{2.38}$$

$$\epsilon = A^{-1}\mathbf{z}. \tag{2.39}$$

One can state that $\mathbf{u}$ is the block whitened space time steering vector and $\epsilon$ is the block whitened data vector.

The detection test statistics can be rearranged as [8]

$$l_{MF} = \frac{|(D^{-1/2}\mathbf{u})^H(D^{-1/2}\epsilon)|^2}{|(D^{-1/2}\mathbf{u})^H(D^{-1/2}\mathbf{u})|}. \tag{2.40}$$

The vectors $\mathbf{t}$and $\mathbf{v}$ are defined as

$$\mathbf{t} = D^{-1/2}\mathbf{u}, \tag{2.41}$$

$$\mathbf{v} = D^{-1/2}\epsilon. \tag{2.42}$$

The final form of the detection test statistics is

$$l_{MF} = \frac{|\mathbf{t}^H\mathbf{v}|^2}{|\mathbf{t}^H\mathbf{t}|} = \frac{|\sum_{n=0}^{N-1}\mathbf{t}^H(n)\mathbf{v}(n)|^2}{|\sum_{n=0}^{N-1}\mathbf{t}^H(n)\mathbf{t}(n)|} \tag{2.43}$$

where $\mathbf{t}(n)$ and $\mathbf{v}(n)$ are vectors of size $M$ x 1 which corresponds to the elements of vectors $\mathbf{t}$ and $\mathbf{v}$ for the $n$th pulse.

The inverse of the lower-block triangular matrix $A$ will be denoted as

$$A^{-1} = \begin{bmatrix} A_1^H(1) & 0 & \dots & 0 \\ A_2^H(2) & A_2^H(1) & \dots & 0 \\ \vdots & \vdots & \ddots & \vdots \\ A_N^H(N) & A_N^H(N-1) & \dots & A_N^H(1) \end{bmatrix} \tag{2.44}$$

where $A_n^H(k)$ are matrices of size $M$ x $M$ and $A_n^H(1)$ are the identity matrices of size $M$ x $M$.

Element of $\epsilon$ and $v$ can be found by the following equations

$$\epsilon(n) = \sum_{k=1}^{n} A_n^H(k)\mathbf{z}(n-k+1) \quad , \qquad n = 1, 2, \dots, N \tag{2.45}$$

$$\mathbf{v}(n) = D^{-1/2}(n)\epsilon(n) \quad , \qquad n = 1, 2, \dots, N \tag{2.46}$$

where $\mathbf{z}(n)$ are vectors of size $M$ x 1 that contains the data sampled at each antenna array output for the $n$th pulse.

Under no target hypothesis $H_0$, the signal $v$ is equal to $v_u$ whose covariance is

$$E\{\mathbf{v}_u\mathbf{v}_u^H\} = E\{D^{-1/2}\epsilon_u\epsilon_u^H D^{-1/2}\} = E\{D^{-1/2}A^{-1}\mathbf{z}_u\mathbf{z}_u^H A^{-H}D^{-1/2}\}, \tag{2.47}$$

$$E\{\mathbf{v}_u\mathbf{v}_u^H\} = D^{-1/2}A^{-1}E\{\mathbf{z}_u\mathbf{z}_u^H\}A^{-H}D^{-1/2} = D^{-1/2}A^{-1}R_uA^{-H}D^{-1/2}, \tag{2.48}$$

$$E\{\mathbf{v}_u\mathbf{v}_u^H\} = D^{-1/2}A^{-1}ADA^HA^{-H}D^{-1/2} = I \tag{2.49}$$

where $\mathbf{z}_u$ is the data vector under no target hypothesis $H_0$.

One can state that $\mathbf{v}$ has a zero-mean distribution with identity covariance. The filter coefficients in the $A^{-1}$accomplishes the block whitening and the matrix $D^{-1/2}$ is used for the block variance normalization [8]. Parametric adaptive matched filtering technique will be built by assuming the LDU decomposition of interference covariance matrix has a certain structure.

### 2.7.2 PAMF Interference Model

Parametric adaptive matched filtering technique is built on the assumption that $\mathbf{z}_u$ can be estimated with forward auto-regressive filter parameters of degree $p$ as [8]

$$\hat{\mathbf{z}}(n) = -\sum_{k=2}^{p+1} A_f^H(k)\mathbf{z}_u(n-k+1) \quad , \qquad n = p+1, p+2, \ldots, N \tag{2.50}$$

The estimation error $z_\epsilon$ of the estimator described in (2.50) is

$$\mathbf{z}_\epsilon(n) = \mathbf{z}_u(n) - \hat{\mathbf{z}}(n) = \sum_{k=1}^{p+1} A_f^H(k)\mathbf{z}_u(n-k+1) \quad , \quad n = p+1, p+2, \ldots, N-p \tag{2.51}$$

given that $A_f^H(1)$ is the identity matrix of size $M$ x $M$.

Comparing equations (2.45) and (2.51), two assumptions of the PAMF method can be observed. First assumption is that the filter parameters $A_n^H(k)$ are independent of time.

$$A_n^H(k) = A_f^H(k) \quad , \quad n < p+2 \tag{2.52}$$

The second assumption is that the correlation between pulses that have more than $p+1$ pulses are neglected. In return, the dimensionality of the problem is decreased.

$$A_n^H(k) = 0 \quad , \quad n > p+1 \tag{2.53}$$

However, if the correlations between the pulses that are neglected, are high, the estimation error will increase. Also, the coherent processing gain is decreased to $N-p$ instead of $N$.

The estimation error elements $\mathbf{b}_\epsilon(n)$ obtained when the input is the space time target steering vector is

$$\mathbf{b}_\epsilon(n) = \sum_{k=0}^{p} A_f^H(k)\mathbf{b}(n-k+p) \quad , \qquad n = 0, 1, \ldots, N-p-1 \tag{2.54}$$

where $\mathbf{b}(n)$ are vectors of size $M$ x 1 that contains the space time target steering vector elements at each antenna array output for the $n$th pulse.

In order to express the transformations in canonical form, the matrix $B$ is formed as,

$$B = \begin{bmatrix} A_f^H(p+1) & A_f^H(p) & \ldots & A_f^H(1) & 0 & \ldots & \ldots & \ldots & 0 \\ 0 & A_f^H(p+1) & A_f^H(p) & \ldots & A_f^H(1) & 0 & & & 0 \\ 0 & 0 & \ddots & \ddots & & \ddots & & & \vdots \\ \vdots & \vdots & \ddots & \ddots & \ddots & & \ddots & & \vdots \\ \vdots & \vdots & & \ddots & \ddots & \ddots & & A_f^H(1) & 0 \\ 0 & 0 & \ldots & \ldots & 0 & A_f^H(p+1) & A_f^H(p) & \ldots & A_f^H(1) \end{bmatrix}. \tag{2.55}$$

In the canonical form the error expressions become,

$$z_\epsilon = B\mathbf{z}_u, \tag{2.56}$$

$$b_\epsilon = B\mathbf{b}. \tag{2.57}$$

After the PAMF filter coefficient estimation, these matrices will be used for determining weighting vector calculation.

### 2.7.3 PAMF Filter Coefficient Determination

The filter parameters $A_f^H(k)$ can be determined by least squares method. The filter parameters are chosen such that the estimation error is minimized [8]. Note that $A_f^H(1)$ is assumed to be $I_M$ which is the identity matrix of size $M$ x $M$.

$$A_f^H(k) = \underset{A_f^H(k)}{argmin}(E\{z_\epsilon^H z_\epsilon\}). \tag{2.58}$$

In order to determine the filter parameters, the interference covariance matrix $R_u$ is required. Since the interference covariance matrix is unknown, diagonally-loaded sample matrix (DL-SM) method described in (2.26) is used. Using the estimated interference covariance matrix $\hat{R}_u$, the following simultaneous equations are to be solved.

$$\frac{\partial}{\partial A_f^H(k)} z_\epsilon^H z_\epsilon = 0 \quad , \quad k = 2, 3, \ldots, p+1 \tag{2.59}$$

Equation (2.59) is solved in [9]. The filter coefficients are found using $R_f$ which is defined as

$$R_f = \sum_{k=1}^{N-p} \hat{R}_u(k : k+p) \tag{2.60}$$

where $\hat{R}_u(k : k+p)$ is a $(p+1)M$ x $(p+1)M$ sized matrix that corresponds to the correlations of the $k$th and $(k+p)$th pulses. $R_f$ can be divided into four sub-matrices as

$$R_f = \begin{bmatrix} R_{ff} & R_{f1} \\ R_{10} & R_{11} \end{bmatrix} \tag{2.61}$$

where $R_{ff}$ is a $pM$ x $pM$ sized matrix, $R_{f1}$ is a $pM$ x $M$ sized matrix, $R_{10}$ is a $M$ x $M$ sized matrix and $R_{11}$ is a $M$ x $M$ sized matrix. Using these sub-matrices, the PAMF filter matrices are derived as

$$A_f = \begin{bmatrix} A_f(p+1) \\ A_f(p) \\ \vdots \\ A_f(2) \\ A_f(1) \end{bmatrix} = \begin{bmatrix} -R_{ff}^{-1} R_{f1} \\ I_M \end{bmatrix}. \tag{2.62}$$

### 2.7.4 PAMF Weighting Vector Calculation

In order to obtain the weighting vector, time averaged $p$th order PAMF filtered covariance matrix is defined as

$$R_{f\epsilon} = \frac{1}{N-p} A_f^H R_f A_f. \tag{2.63}$$

Then the estimated covariance matrix inverse is

$$R_{PAMF}^{-1} = B^H (I_{N-p} \otimes R_{fe}^{-1}) B \tag{2.64}$$

where $\otimes$ denotes the Kronecker product and $B$ is defined as in (2.55).

The matched filter coefficients can be expressed as [9]

$$W_{PAMF} = R_{PAMF}^{-1}\mathbf{b} \tag{2.65}$$

where $\mathbf{b}$ is the space-time target steering vector. Then the final form of the detection test statistics is

$$l_{PAMF} = \frac{\left|\mathbf{b}^H R_{PAMF}^{-H}\mathbf{z}\right|^2}{\left|\mathbf{b}^H R_{PAMF}^{-H}\mathbf{b}\right|}, \tag{2.66}$$

$$l_{PAMF} = \frac{\left|\mathbf{W}_{PAMF}^H\mathbf{z}\right|^2}{\left|\mathbf{W}_{PAMF}^H\mathbf{b}\right|}. \tag{2.67}$$

# CHAPTER 3

# SPACE TIME AUTO-REGRESSIVE FILTERING

## 3.1 Auto-Regressive Structured Interference Modeling

Space Time Auto-Regressive (STAR) Filtering is an alternative to partially adaptive STAP for reducing the dimension of the clutter covariance estimation problem. STAR filtering method constructs an auto-regressive (AR) model to estimate the interference. In essence, STAR makes use of a vector AR model of order $p$, estimated from secondary data to construct a structured subspace that is as orthogonal to the interference subspace as possible.

The auto-regressive model followed by the unwanted interference signal components at range bin $k$ for a system with $M$ antenna array elements and $N$ pulses in a coherent processing interval is assumed to be as follows [10] [1]

$$\sum_{i=0}^{p-1} \mathbf{A_i} \mathbf{z}_{u,k}(n+i) = \mathbf{0_{M'x1}} \quad , \qquad n = 1, \ldots, N-p+1 \tag{3.1}$$

where

- $\mathbf{z}_{u,k}(n)$ is a $M$x1 vector and the elements of $\mathbf{z}_{u,k}(n)$ corresponds to the data sampled at each array output for the $k$th secondary range bin at the pulse $n$. The data at $k$th secondary range bin are assumed to be only composed of interference signal
- $\mathbf{A_i}$ are matrix filter taps of size $M'$x$M$ and the coefficients of $\mathbf{A_i}$ are to be determined from the secondary data.
- The filter order parameters $p$ and $M'$ are unknown and they are to be determined from the data or a data model beforehand. In this section determination of these parameters will be covered.

One can observe that the model suggested in (3.1) only accounts for the correlation between $p$ consecutive pulses since the model only uses $p$ filter taps to null the interference clutter. Therefore the dimension of the problem in the slow time is reduced and similarly the amount of the secondary range bins to estimate the interference covariance matrix are fewer. However if the correlations between the pulses that are neglected, are actually high, performance of the interference suppression will decrease. Another observation that can be made is that the matrix filter taps $\mathbf{A_i}$ are time independent which means that the correlation between $p$ consecutive pulses are assumed to be the same for all the pulses in the coherent processing interval. This property of the model improves the estimation of the matrix filter taps $\mathbf{A_i}$. However, if the variation of the correlations between $p$ consecutive pulses change, than the performance of the interference suppression will again decrease. The assumptions in (3.1) imposes a structure on the interference covariance matrix, therefore fewer secondary data are required

[1] Equation (3.1) actually means minimizing the norm of the left hand side.

for estimation. This phenomenon is useful in situations where fewer secondary samples are available due to non-homogeneity.

Unlike other vector error prediction filters, filter matrix coefficients $\mathbf{A_i}$ are not assumed to be square and the leading coefficient $\mathbf{A_0}$ is not assumed to be identity matrix. These design choices allow for more freedom in matching the interference subspace and allow the spatial correlation structure to be accounted for in the same step as the temporal correlation [11]. Therefore spatial and temporal whitening occurs in one stage.

## 3.2 Filter Coefficient Determination

In order to state the filter coefficient determination problem in canonical form, it is convenient to define the following

$$\varepsilon_{\mathbf{k}} = \begin{bmatrix} \mathbf{z}_{u,k}(1) & \cdots & \mathbf{z}_{u,k}(N-p+1) \\ \vdots & & \vdots \\ \mathbf{z}_{u,k}(p-1) & \cdots & \mathbf{z}_{u,k}(N) \end{bmatrix}, \tag{3.2}$$

where $\varepsilon_{\mathbf{k}}$ is a matrix of size $ML$ x (N − p + 1) and it is formed from the data input to the auto-regressive filter for the $k$th secondary range bin.

The matrix $\mathbf{E}$ of size $ML$ x (N − p + 1)$K$ that includes all the secondary range bin data can be formed as

$$\mathbf{E} = \begin{bmatrix} \varepsilon_1 & \varepsilon_2 & \cdots & \varepsilon_{K-1} & \varepsilon_K \end{bmatrix} \tag{3.3}$$

where $K$ is the total number of secondary range bins used.

The matrix filter $\mathbf{A^H}$ of size $M'$ x $LM$ will be denoted as

$$\mathbf{A^H} = \begin{bmatrix} A_0 & A_1 & \ldots & A_{(p-2)} & A_{(p-1)} \end{bmatrix}. \tag{3.4}$$

The matrix filter bank $\mathbb{A}^{\mathrm{H}}$ of size $M'(N-p+1)$ x $MN$ will be denoted as

$$\mathbb{A}^{\mathrm{H}} = \begin{bmatrix} A_0 & A_1 & \cdots & A_{(p-1)} & 0 & \ldots & \ldots & \ldots & 0 \\ 0 & A_0 & A_1 & \cdots & A_{(p-1)} & 0 & & & 0 \\ 0 & 0 & \ddots & \ddots & & \ddots & & & \vdots \\ \vdots & \vdots & \ddots & \ddots & \ddots & & \ddots & & \vdots \\ \vdots & \vdots & & \ddots & \ddots & \ddots & & \ddots & 0 \\ 0 & 0 & \ldots & \ldots & 0 & A_0 & A_1 & \cdots & A_{(p-1)} \end{bmatrix}. \tag{3.5}$$

The secondary data set for the $k$th secondary range bin $\mathbf{z}_{u,k}$ is a $MN$ x 1 vector as

$$\mathbf{z}_{u,k} = \begin{bmatrix} \mathbf{z}_{u,k}(1) \\ \mathbf{z}_{u,k}(2) \\ \vdots \\ \mathbf{z}_{u,k}(N-1) \\ \mathbf{z}_{u,k}(N) \end{bmatrix}. \tag{3.6}$$

Now, (3.1) can be rewritten as

$$\mathbf{A}^H \varepsilon_{\mathbf{k}} = \mathbf{0}_{\mathbf{M'x}(\mathrm{N-p+1})} \tag{3.7}$$

and

$$\mathbf{A}^H\mathbf{E} = \mathbf{0}_{\mathbf{M'x(N-p+1)K}} \tag{3.8}$$

and

$$\mathbb{A}^{\mathrm{H}}\mathbf{z}_{u,k} = \mathbf{0}_{\mathbf{M'(N-p+1)x1}}. \tag{3.9}$$

Due to mismodelling and noise, the equalities in (3.8),(3.7),(3.9) usually does not hold in practice. Therefore $\mathbf{E}$ is usually full rank and has no true nullspace. The residual error $\epsilon$ is defined as

$$\mathbf{A}^H\mathbf{E} = \epsilon. \tag{3.10}$$

The filter coefficients that minimizes the residual error $\epsilon$ is desired. Therefore the filter coefficients are determined by the least squares method [10].

$$\mathbf{A} = \underset{\mathbf{A}}{argmin}\left(\left\|\mathbf{A}^H\mathbf{E}\right\|^2\right). \tag{3.11}$$

To avoid a trivial solution, the constraint $\mathbf{A^H A} = \mathbf{I}$ is used. Since $\mathbf{A}_i$ are assumed to be matrices of size $M' \times M$, the solution to the problem described in (3.11) under the constraint $\mathbf{A^H A} = \mathbf{I}$, is $M'$ left singular vectors of the matrix $\mathbf{E}$ which correspond to the smallest singular values. The left singular vectors of the $\mathbf{E}$ can be found by finding the eigenvalues of the matrix $\mathbf{E^H E}$. The left singular vectors that have the smallest singular values are the ones with the smallest eigenvalues of $\mathbf{E^H E}$.

## 3.3 Model Order Estimation

The biggest difficulty faced with the use of the parametric model is determining the model order that results in best performance. The parametric model presented requires two parameters to be chosen: $M'$ and $p$. Two well known criteria for choosing autoregressive model orders for scalar (AR) processes is the minimum description length (MDL) criterion [12] and the Akaike information theoretic criterion (AIC) [13]. The approach taken here is to fix $M'$ and use a prediction error criterion to choose $p$. Standard approaches for estimating the order of an AR process calculate the prediction error residual for each candidate model order and then add a penalty term $P$, which accounts for the number of free parameters in the model [11].

$$p = \underset{p}{argmin}\left(\ln\left(\left|\epsilon\epsilon^H\right|\right) - P\right) \tag{3.12}$$

where penalty terms for AIC and MDL are

$$P_{AIC} = \ln\left(K\left(N-p+1\right)\right) - \frac{2pMM' - M'\left(M'+1\right)}{KMN}, \tag{3.13}$$

$$P_{MDL} = \ln\left(K\left(N-p+1\right)\right) - \frac{2pMM' - M'\left(M'+1\right)}{2KMN}\ln\left(KMN\right) \tag{3.14}$$

and $|\cdot|$ denotes the determinant of a matrix.

This procedure is not repeated for every CPI. The model order selection is repeated much less frequently than target detection. Another point that has to be considered is that the secondary data set used for model order estimation should differ from the secondary data set used for filter parameter estimation.

The derivation of the model order selection criteria assumed a fixed $M'$. Under the assumed model, one can observe that the interference is orthogonal to $\mathbb{A}$ from equation (3.9). If the clutter has a rank of $\rho$ , then the rank of $\mathbb{A}$ should be $MN - \rho$ . If $\mathbb{A}$ is full rank, then $M'$ should satisfy [10]

$$M' = \left\lceil \frac{MN - \rho}{N - p + 1} \right\rceil \tag{3.15}$$

where $\lceil \cdot \rceil$ denotes the smallest integer that is larger than the term in the brackets. However the rank of the interference is generally not known a priori. The interference rank can be estimated by using Brennan's rule.

## 3.4 STAR Weighting Vector Calculation

The approach used while obtaining the detection test statistics is prediction error filtering. In (3.1) a model for prediction of the interference was developed. In the presence of a target, the residual error defined in (3.10) will increase since the matrix filter $\mathbf{A}$ is matched to the subspace that is orthogonal to the clutter but not to the target steering vector. The detection test statistics aim to match the filter residual error with the residual error that would be obtained in the presence of a target that has a space-time target steering vector $\mathbf{b}$. The matched filter coefficients can be expressed as [11]

$$W_{PMF} = \mathbb{A}\mathbb{A}^{\mathbf{H}}\mathbf{b} \tag{3.16}$$

where $\mathbf{b}$ is the space-time target steering vector of size $MN$ x 1.

Then, the final form of the detection test statistics is

$$l_{STAR} = \frac{\left|\mathbf{b}^H \mathbb{A}\mathbb{A}^H \mathbf{z}\right|^2}{\mathbf{b}^H \mathbb{A}\mathbb{A}^H \mathbf{b}} \tag{3.17}$$

where $\mathbf{z}$ is the data vector that corresponds to the range bin under test and $\mathbf{z}$ is a vector of size $MN$ x 1 such as

$$\mathbf{z} = \begin{bmatrix} \mathbf{z}(1) \\ \mathbf{z}(2) \\ \vdots \\ \mathbf{z}(N-1) \\ \mathbf{z}(N) \end{bmatrix} \tag{3.18}$$

where $\mathbf{z}(n)$ is an $M$x1 vector and the elements of $\mathbf{z}(n)$ corresponds to the data sampled at each array output for the range bin under test at the pulse $n$.

The computational load of STAR filtering can be approximated as the sum of computations required for filter parameter determination and weight vector determination.

The prediction error weight vector requires $O(2M'ML(N - p + 1))$ flops to compute. To find the left singular vectors of an $A$ x $B$ matrix ( where $B > A$ ) requires $O(A^2B)$ flops, therefore filter parameter determination requires $O((ML)^2(N - p + 1)K)$ flops to compute. The computational complexity of the STAR algorithm can be estimated as

$$STAR_{flop} = O((ML)^2(N - p + 1)K) + O(2M'ML(N - p + 1)). \tag{3.19}$$

# CHAPTER 4

# MODEL BASED GMTI

Adaptive STAP approaches estimate the clutter covariance matrix using secondary data. However, the clutter covariance matrix for a known GMTI geometry is not completely unknown. Using the geometry of the data acquisition and estimating certain clutter characteristics, clutter covariance matrix can be estimated. In order to suppress the clutter, the Model Based GMTI approach constructs a model for the clutter covariance matrix. This section investigates a model-based GMTI approach by introducing a clutter covariance model together with clutter power estimation. Clutter power estimation performance is to be investigated under non-homogenous clutter environments with discrete clutter and clutter transition areas. Non-homogeneity detection and intelligent power estimation techniques are to be used for improving clutter power estimation performance.

## 4.1 Clutter Covariance Model

A clutter covariance matrix model for side-looking GMTI geometry was developed by Prof. Dr. Yalçın Tanık [25]. This subsection introduces the model suggested. In the model following assumptions were made:

- The area illuminated by the antenna beam is flat.
- Clutter scatterer points are statistically independent.
- Inter-clutter motion is not present.
- Distance traveled during a coherent processing interval is much less than the range
- Maximum distance between receive antenna phase centers is much less than the range

The geometry assumed for the GMTI data acquisition is shown in Figure (4.1).

A platform with velocity $v$ moving in the $x$ direction is assumed. The platform height from the ground is $h$. The point zero is the initial position of the platform. $n$ and $k$ corresponds to the platform positions at the $n$th and $k$th pulses. The line that has $\phi$ degrees from the platform velocity direction corresponds to the axis that the antenna phase centers are mounted. Transmitter antenna is assumed to be at the center and the receiver antennas are assumed to be located with equal distance to each other on the line. The distance between the receiver antennas is $L$. Contribution of the ground point $(x, y)$ to clutter component of the data sampled at the $i$th antenna at the $n$th pulse can be expressed as:

$$c_{in}(x,y) = \frac{\alpha}{r_n^T r_n^i} G_T^V\left(\phi_n^T\right) G_i^V\left(\phi_n^i\right) c(x,y)\, exp\left[-j\frac{2\pi}{\lambda}\left(r_n^T + r_n^i\right)\right] \tag{4.1}$$

where,

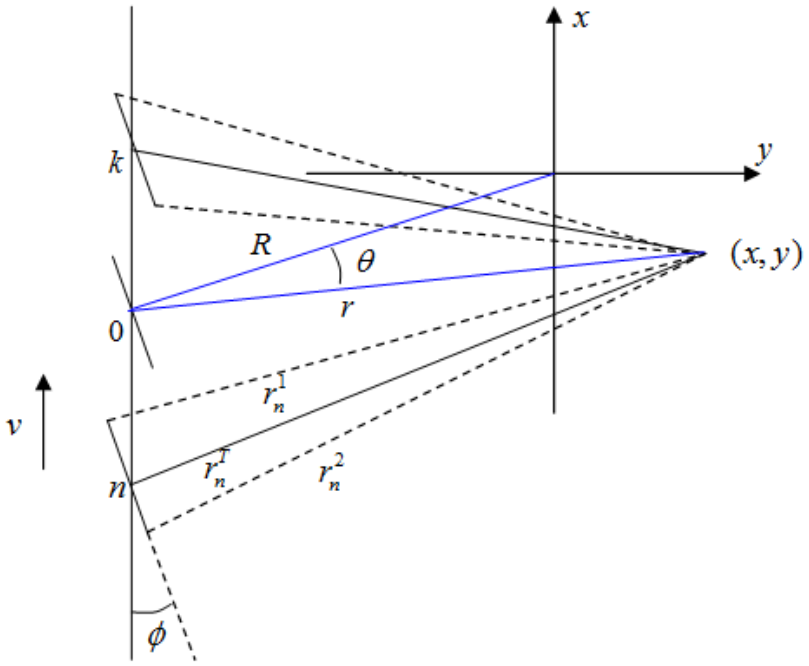


Figure 4.1: GMTI Geometry for Covariance Model [25]

$G_T^V$ : Transmitter antenna voltage pattern,

$\phi_T^V$ : Azimuth angle between the antenna axis and the line that intersects the transmitter antenna center and the point $(x, y)$,

$G_i^V$ : $i$th receiver antenna voltage pattern,

$\phi_n^i$ :Azimuth angle between the antenna axis and the line that intersects the $i$th receiver antenna center and the point $(x, y)$,

$r_n^T$ : Distance between the point $(x, y)$ and the transmitter antenna center ,

$r_n^i$ : Distance between the point $(x, y)$ and the $i$th receiver antenna center,

$\alpha$ : Radar equation coefficient.

Clutter back-scatter coefficients are assumed to be independent from each other:

$$E\left\{c\left(x,y\right)c^{*}(x',y')\right\}=\sigma_c^2\left(x,y\right)\delta\left(x-x',y-y'\right) \tag{4.2}$$

where $\sigma_c^2\left(x,y\right)$ is the mean radar cross section at ground point $(x, y)$ and $\delta(\cdot)$ represents the impulse function.

The cross-covariance between the pulses and the antennas is the integral of the single point contribution over the illuminated area so that

$$E\left\{c_{in}c_{mk}^{*}\right\}=\iiiint E\left\{c_{in}\left(x,y\right)c_{mk}^{*}\left(x',y'\right)\right\}dxdydx'dy'. \tag{4.3}$$

Using (4.1), (4.2) and (4.3), one can rewrite (4.3) as :

$$E\left\{c_{in}c_{mk}^{*}\right\} = \iint \frac{\alpha^2}{r_n^T r_n^i r_k^T r_k^m} E\left\{\sigma_c^2(x,y)\right\} G_T^V\left(\phi_n^T\right) G_l^V\left(\phi_n^i\right) \tag{4.4}$$

$$G_T^{V*}\left(\phi_k^T\right) G_m^{V*}\left(\phi_k^m\right) exp\left[-j\frac{2\pi}{\lambda}\left(r_n^T + r_n^i - r_k^T - r_k^m\right)\right] dxdy. \tag{4.5}$$

If the ground range which is the distance between platform nadir point to the point $(x, y)$, is denoted by $r'$, one can write the equations (4.6), (4.7) and (4.8).

$$dxdy = r'd\theta dr' \tag{4.6}$$

$$r' = \sqrt{r^2 - h^2} \tag{4.7}$$

$$rdr = r'dr' \tag{4.8}$$

By changing variables, (4.5) can be rewritten as:

$$E\left\{c_{in}c_{mk}^{*}\right\} = \iint \frac{\alpha^2}{r_n^T r_n^i r_k^T r_k^m} E\left\{\sigma_c^2(x,y)\right\} G_T^V\left(\phi_n^T\right) G_l^V\left(\phi_n^i\right) \tag{4.9}$$

$$G_T^{V*}\left(\phi_k^T\right) G_m^{V*}\left(\phi_k^m\right) exp\left[-j\frac{2\pi}{\lambda}\left(r_n^T + r_n^i - r_k^T - r_k^m\right)\right] drd\theta.$$

The initial ground range of the radar $R'$ can be described as

$$R' = \sqrt{R^2 - h^2} \tag{4.10}$$

where $R$ is the initial range.

Using equation (4.10), initial position can be written as

$$x_0 = -R'sin\phi, \tag{4.11}$$

$$y_0 = -R'cos\phi \tag{4.12}$$

and the coordinates of the point $(x, y)$ is

$$x = x_0 + r'sin\left(\phi - \theta\right), \tag{4.13}$$

$$y = -r'cos\left(\phi - \theta\right). \tag{4.14}$$

Using the cosine law, one can write that

$$(r_n^{T'})^2 = (n\triangle x)^2 + r'^2 + 2n\triangle xr'cos\left(90^\circ - \theta + \phi\right) \tag{4.15}$$

and

$$(r_n^T)^2 = (n\triangle x)^2 + r^2 + 2n\triangle xr'sin\left(\theta - \phi\right) \tag{4.16}$$

where $\triangle x$ is the distance hte platform traveles between two consecutive pulses.

The relation between $r'$,$r$ and $h$ is

$$r^2 = r'^2 + h^2. \tag{4.17}$$

On the other hand, from equations (4.18) and (4.19), $\theta_n$variable can be found.

$$sin\left(\theta_n - \phi\right) = \frac{(n\triangle x)^2 + (r_n^T)^2 - r^2}{2\left(n\triangle x\right) r_n^{T'}}, \tag{4.18}$$

$$sin\left(\theta_n - \phi\right) = \frac{n\triangle x + r' sin\left(\theta - \phi\right)}{r_n^{T'}}. \tag{4.19}$$

Finally,

$$\left(r_n^1\right)^2 = \left(r_n^T\right)^2 + (L/2)^2 + L r_n^{T'} sin\theta_n, \tag{4.20}$$

$$\left(r_n^2\right)^2 = \left(r_n^T\right)^2 + (L/2)^2 - L r_n^{T'} sin\theta_n. \tag{4.21}$$

It was previously assumed that the distance traveled during a coherent processing interval and the maximum distance between receive antenna phase centers are much less than the range, the range $r$ is relatively constant in a single range bin.

$$r_n^T \cong r, \tag{4.22}$$

$$r_n^i \cong r, \tag{4.23}$$

$$\phi_n^T \cong \theta, \tag{4.24}$$

$$\phi_n^i \cong \theta, \tag{4.25}$$

$$\theta_n \cong \theta. \tag{4.26}$$

With these approximations, (4.9) can be rearranged as,

$$\begin{aligned} E\left\{c_{in}c_{mk}^*\right\} \cong \quad & \iint \tfrac{\alpha^2}{r^3} E\left\{\sigma_c^2(x,y)\right\} G_T^V(\theta)\, G_l^V(\theta)\, G_T^{V*}(\theta)\, G_m^{V*}(\theta) \\ & exp\left[-j\tfrac{2\pi}{\lambda}\left(r_n^T + r_n^i - r_k^T - r_k^m\right)\right] dr d\theta. \end{aligned} \tag{4.27}$$

One can write the following expressions in order to calculate the range difference

$$r_n^T \cong r + \frac{n\triangle x r'}{r} sin\left(\theta - \phi\right), \tag{4.28}$$

$$r_n^T - r_k^T \cong r + \frac{(n-k)\triangle x r'}{r} sin\left(\theta - \phi\right). \tag{4.29}$$

With a similar approach,

$$r_n^1 \cong r_n^T + \frac{L r_n^{T'}}{r_n^T} sin\theta, \tag{4.30}$$

$$r_n^2 \cong r_n^T - \frac{L r_n^{T'}}{r_n^T} sin\theta \tag{4.31}$$

is obtained. Therefore,

$$r_n^i - r_k^m \cong \frac{n\triangle x r'}{r} sin\left(\theta - \phi\right) + L sin\theta \left[\rho_i \frac{r_n^{T'}}{r_n^T} - \rho_m \frac{r_k^{T'}}{r_k^T}\right] \tag{4.32}$$

where, $\rho_1 = 1, \rho_2 = -1$ and $\frac{r_k^{T'}}{r_k^T} \cong \frac{r'}{r}$.

As a result:

$$r_n^i - r_k^m \cong \frac{r'}{r}\left[(n-k)\triangle x sin\left(\theta - \phi\right) + \left(\rho_i - \rho_m\right) L sin\theta\right]. \tag{4.33}$$

Transmitter-Receiver voltage pattern is defined as

$$G_m(\phi) = G_T^V(\phi)\, G_m^V(\phi). \tag{4.34}$$

Equation (4.9) can be rearranged as,

$$E\left\{c_{in}c_{mk}^*\right\} \cong \iint \frac{\alpha^2}{r^3} E\left\{\sigma_c^2(x,y)\right\} G_l(\theta)\, G_m^*(\theta) \; exp\left[-j\frac{2\pi r}{\lambda r'}\left(2(n-k)\triangle x sin(\theta-\phi) + L(\rho_i-\rho_m)\, sin\theta\right)\right] \; drd\theta. \tag{4.35}$$

Under the assumption that antenna beamwidths are small,

$$sin(\theta-\phi) \cong \theta cos\phi - sin\phi. \tag{4.36}$$

Equation (4.9) can be rearranged as,

$$E\left\{c_{in}c_{mk}^*\right\} \cong \frac{\alpha^2}{r^3} exp\left[j\frac{4\pi\beta(n-k)\triangle x sin\phi}{\lambda}\right] \iint \sigma_c^2(x,y)\, G_l(\theta)\, G_m^*(\theta) \; exp\left[-j\frac{2\pi\beta}{\lambda}\left(2(n-k)\triangle x cos(\phi) + L(\rho_i-\rho_m))\,\theta\right]\right] drd\theta \tag{4.37}$$

where $\beta$ is defined as

$$\beta = \frac{r'}{r} = \frac{\sqrt{r^2-h^2}}{r}. \tag{4.38}$$

If the clutter is homogeneous ,

$$E\left\{\sigma_c^2(x,y)\right\} = \sigma_0 \tag{4.39}$$

and range resolution is small, (4.9) can be put into following form :

$$E\left\{c_{in}c_{mk}^*\right\} \cong \frac{\alpha^2\sigma_0\triangle r}{r^3} exp\left[j\frac{4\pi\beta(n-k)\triangle x sin\phi}{\lambda}\right] \int G(\theta)\, G_m^*(\theta)\, exp\left[-j\frac{2\pi\beta}{\lambda}\left(2(n-k)\triangle x cos(\phi) + L(\rho_i-\rho_m))\,\theta\right]\right] d\theta. \tag{4.40}$$

The radar equation coefficient can be formed as

$$\alpha^2 = \frac{\lambda^2 L_T}{(4\pi)^3} P_T T_P \tag{4.41}$$

where $\lambda$ is the wavelength, $L_T$ is the transmitter loss, $P_T$ is the transmitted power. The only unknown parameter that is to be estimated from data is the specific mean radar cross section of the clutter $\sigma_0$.

## 4.2 Space Time Target Steering Vector Model

Space time target steering vector can be obtained similar to the clutter covariance matrix. The distance traveled by the target is assumed to be much less than its range. Therefore, $\theta$ is approximately constant during a coherent processing interval. However, changes in range due to the target radial velocity need to be considered.

The signal component for the target echo for the *n*th pulse at the *i*th antenna array element can be expressed as

$$b_{i,n} = \frac{\alpha}{r_n^T r_n^i} G_T^V\left(\phi_n^T\right) G_l^V\left(\phi_n^i\right) \sigma_s exp(-j\frac{2\pi}{\lambda}(r_n^T + r_n^i)) \tag{4.42}$$

where $\sigma_s^2$ is the mean radar cross section of the target. Since the target is not stationary, range values are updated as

$$r_n^T = r + n\Delta r + n\beta\Delta x' \sin(\theta - \phi), \tag{4.43}$$

$$r_n^i \cong r_n^T - \rho_i \beta L \sin(\theta) \tag{4.44}$$

where $\Delta r$ is the distance traveled in the range direction by the target between two consecutive pulses, while $\Delta x'$ is the distance traveled in the cross-range direction by the target between two consecutive pulses.

The signal component for the target echo for the $n$th pulse at the $i$th antenna array element can be updated as

$$b_{i,n} = \frac{\alpha}{r_n^T r_n^i} G_T^V\left(\phi_n^T\right) G_l^V\left(\phi_n^i\right) \sigma_s exp(-j\frac{2\pi}{\lambda}(r + n(\Delta r + \beta\Delta x' \sin(\theta - \phi)) - \rho_i \beta L \sin(\theta))). \tag{4.45}$$

## 4.3 Clutter Power Estimation

As indicated in the previous subsection, in order to model the clutter covariance matrix under the given assumptions, the only parameter that is to be estimated from the secondary data is the mean radar cross section of the clutter $\sigma_0$. The estimation is based on the assumption that the clutter power is identical to the clutter power in the secondary range bins. Defining $\mathrm{z}_{in,k}$ as the data sampled at the $i$th antenna at the pulse $n$ for the $k$th secondary range bin, $\mathrm{z}_{in,k}$ are assumed to be only composed of interference signal.

$$\mathrm{z}_{in,k} = c_{in,k} + n_{in} \tag{4.46}$$

where $c_{in,k}$ is the clutter component and $n_{in}$ is the thermal noise component.

Clutter power estimation is to be accomplished by integrating the instantaneous power of $\mathrm{z}_{in,k}$ which is [15]

$$y_{i,k} = \sum_{n=1}^{N} \mathrm{z}_{in,k} \mathrm{z}_{in,k}^* \tag{4.47}$$

where $N$ is the total number of pulses in a coherent processing interval. The expected value of the $y_{i,k}$is

$$E\left\{y_{i,k}\right\} = \sum_{n=1}^{N} E\left\{\mathrm{z}_{in,k} \mathrm{z}^{\star}{}_{in,k}\right\}. \tag{4.48}$$

Since $n_{in}$ is white Gaussian, expected value of the $y_{i,k}$ can be expressed as

$$E\left\{y_{i,k}\right\} = \sum_{n=1}^{N} E\left\{\mathrm{c}_{in,k} \mathrm{c}_{in,k}\right\} + E\left\{\mathrm{n}_{in,k} \mathrm{n}_{in,k}\right\}. \tag{4.49}$$

If the termal noise power of the system is $\sigma_n^2$, using (4.40):

$$E\left\{y_{i,k}\right\} = N\frac{\alpha^2 \sigma_0 \triangle r}{r^3} \int G_i(\theta) G_i^*(\theta) \, d\theta + N\sigma_n^2. \tag{4.50}$$

Then the mean clutter radar cross section $\sigma_0$ can be estimated as

$$\widehat{\sigma}_0 = \frac{r^3 \left( -N\sigma_n^2 + \frac{1}{K} \sum_{n=1}^{K} y_{i,k} \right)}{N\alpha^2 \triangle r \int G_i(\theta) G_i^*(\theta) \, d\theta} \tag{4.51}$$

where $K$ is the total number of secondary range bins used in the estimation. Defining $\gamma$ as

$$\gamma = \frac{r^3}{N\alpha^2 \triangle r \int G_i(\theta) G_i^*(\theta) \, d\theta} \tag{4.52}$$

equation (4.51) can be written as

$$\widehat{\sigma}_0 = -\gamma N\sigma_n^2 + \frac{\gamma}{K} \sum_{n=1}^{K} y_{i,k}. \tag{4.53}$$

It should be noted that since the estimated clutter power is obtained by statistical data in (4.53), the estimator may yield a negative power. In such a case, $\sigma_0$ should be taken as zero in practice.

## 4.4 Clutter Power Estimation Under Non-homogeneity

Clutter power estimation described in the previous sub-section was based on the assumption that the clutter power is identical to the clutter power in the secondary range bins. In practice, non-homogeneities may occur due to targets in the secondary samples, clutter edge enviroment or discrete clutter patches. In order to deal with these non-homogeneities, two different approaches will be introduced in this sub-section, nameley inner product Non-homogeneity Detector and an adaptation of the Intelligent CFAR.

### 4.4.1 Inner Product NHD

The inner product NHD does not represent a general approach for nonhomogeneity detection problem. In other words, its value remains limited to specific instances which may be routinely violated in practice. Despite the fact that the method only deals with the instantaneous power integrals, method is called Inner Product NHD in the literature.

The instantaneous power integral was previously defined by (4.47). The expected value of the instantaneous power integral was defined by (4.48). One may observe that the expected value of the instantaneous power integral is the sum of diagonal elements of the secondary data covariance matrix $R_{i,k}$.

$$R_{i,k} = E\left\{ \mathbf{z_{i,k}} \mathbf{z_{i,k}^H} \right\} \tag{4.54}$$

where $\mathbf{z_{i,k}}$ is a $N$ x 1 vector such that

$$\mathbf{z_{i,k}} = \begin{bmatrix} z_{i,1} \\ z_{i,2} \\ \vdots \\ z_{i,(N-1)} \\ z_{i,N} \end{bmatrix}. \tag{4.55}$$

For the clarification of the non-homogeneity problem, two hypotheses are defined for the presence of non-homogeneity as [14]

$$H_h \rightarrow \mathbf{z_{i,k}} = \mathbf{c_h} + \mathbf{n} \tag{4.56}$$

$$H_{nh} \rightarrow \mathbf{z}_{\mathrm{i,k}} = \mathbf{c}_{\mathrm{h}} + \mathbf{c}_{\mathrm{nh}} + \mathbf{n} \tag{4.57}$$

where $\mathbf{c}_h$ denotes the homogeneous clutter echo and $\mathbf{c}_{nh}$ denotes the non-homogeneous clutter echo. It is evident that the non-homogeneous clutter is treated as an addition to the homogeneous clutter. The hypotheses are based on the assumption that the non-homogeneities occur due to discrete clutter or targets in the secondary samples. Inner Product NHD does not account for clutter edge enviroments in the hypothesis construction process.

If the signal received under hypothesis $H_h$ is denoted as $\mathbf{z}_h$, the covariance matrix under different hypothesizes can be denoted as

$$R_h = R_{ch} + \sigma_n^2 I \tag{4.58}$$

$$R_{nh} = R_h + R_{cnh} + R_{cross} + R_{cross}^H \tag{4.59}$$

where

$$R_{cross} = E\left\{\mathbf{c}_{nh}\left(\mathbf{c}_h + \mathbf{n}\right)^H\right\}, \tag{4.60}$$

$$R_{cnh} = E\left\{\mathbf{c}_{nh}\mathbf{c}_{nh}^H\right\}. \tag{4.61}$$

Instantaneous power integral output expected value for the two hypothesis becomes [16]

$$H_h \rightarrow E\left\{y_{i,k}\right\} = trace(R_h), \tag{4.62}$$

$$H_{nh} \rightarrow E\left\{y_{i,k}\right\} = trace(R_h) + trace(R_{cnh} + R_{cross} + R_{cross}^H). \tag{4.63}$$

Since the secondary data covariance matrix is the same for the homogeneous case, instantaneous power integral outputs for homogenous data are expected to be distributed around the expected value given in equation (4.62). Setting upper and lower thresholds on $y_{i,k}$, values outside those bounds are considered nonhomogeneous and the corresponding secondary data are removed.

The instantaneous power integral is a measure of power signal in vector $\mathbf{z}_{i,k}$. However two signal vectors may have similar instantaneous power integrals while having different covariance matrices. Complications arise since data with distinct covariance matrices may have the same mean power, yet possess entirely different off-diagonal covariance matrix elements. Since the NHD will be used for clutter power estimation for the model-based approach, the main interest is the power estimation. Therefore the Inner Product NHD will be considered as an alternative for model-based approach power estimation under clutter in-homogeneity.

### 4.4.2 Intelligent Power Estimation

Intelligent power estimation is an adopted clutter power estimation technique from the Intelligent CFAR method which is proposed in [15]. Intelligent CFAR is a technique that switches to the techniques SO-CFAR, GO-CFAR or CA-CFAR depending on the characteristics of the interference in the secondary data. The aim of the technique is to switch to

- CA-CFAR for homogenous interference
- GO-CFAR at clutter edges
- SO-CFAR at the presence of targets or a discrete clutter patch in the secondary data.

During the clutter power estimation the secondary data is chosen from the neighboring range cells leaving a couple of guard cells. Figure 4.2 shows the selection procedure of secondary data around range data under test. The columns of data matrix corresponds to the same pulse index, while the rows

of the data matrix has the same range value. Red lines are the guard lines, while the yellow line is the line under test which is the line whose clutter power is to be estimated. The lagging window $A$ is a group of secondary data line that has smaller range values than the test line. The leading window $B$ is a group of secondary data line that has larger range values than the test line.

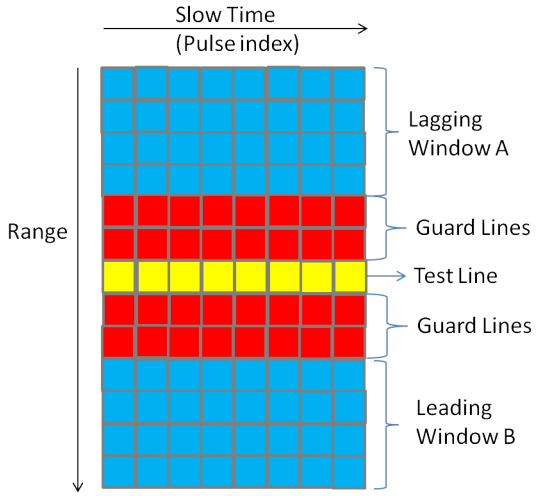


Figure 4.2: Secondary Data Selection for Estimation

The vector that contains the secondary data instantaneous power integrals for the lagging window $\mathbf{y}_A$ is defined as

$$\mathbf{y}_A = \begin{bmatrix} y_{i,1} \\ y_{i,2} \\ \vdots \\ y_{i,(K/2-1)} \\ y_{i,(K/2)} \end{bmatrix} \tag{4.64}$$

where $K$ is the total number of secondary data used for estimation.

The vector that contains the secondary data instantaneous power integrals for the lagging window $\mathbf{y}_B$ is defined as

$$\mathbf{y}_B = \begin{bmatrix} y_{i,(K/2+1)} \\ y_{i,(K/2+2)} \\ \vdots \\ y_{i,(K-1)} \\ y_{i,K} \end{bmatrix}. \tag{4.65}$$

Mean value of the vectors $\mathbf{y}_A$ and $\mathbf{y}_B$ can be found as

$$\mu_A = \frac{2}{K} \sum_{k=1}^{K/2} y_{i,k}, \tag{4.66}$$

$$\mu_B = \frac{2}{K} \sum_{k=K/2+1}^{K} y_{i,k}. \tag{4.67}$$

Vectors $\hat{\mathbf{y}}_A$ and $\hat{\mathbf{y}}_B$ are defined as

$$\hat{\mathbf{y}}_A = \begin{bmatrix} y_{i,1} - \mu_A \\ y_{i,2} - \mu_A \\ \vdots \\ y_{i,(K/2-1)} - \mu_A \\ y_{i,(K/2)} - \mu_A \end{bmatrix}, \tag{4.68}$$

$$\hat{\mathbf{y}}_B = \begin{bmatrix} y_{i,(K/2+1)} - \mu_B \\ y_{i,(K/2+2)} - \mu_B \\ \vdots \\ y_{i,(K-1)} - \mu_B \\ y_{i,K} - \mu_B \end{bmatrix}. \tag{4.69}$$

In order to detect inhomogeneities in the windows due to discrete clutter or targets in the secondary data, the variability index $VI$ [15] is to be used. The variability index statistics for the leading and the lagging window are defined as

$$VI_A = 1 + \frac{\hat{\mathbf{y}}_A^T \hat{\mathbf{y}}_A}{\mu_A^2}, \tag{4.70}$$

$$VI_B = 1 + \frac{\hat{\mathbf{y}}_B^T \hat{\mathbf{y}}_B}{\mu_B^2}. \tag{4.71}$$

Distribution of the $VI$ is independent of the clutter power in a homogeneous environment, but varies considerably in the presence of discrete clutter or targets in the secondary data within the used window. The $VI$ is compared with a threshold $K_{VI}$ to determine if the lines with which the $VI$ is computed are from a homogeneous environment or from a non-homogeneous environment using the following hypothesis test:

$$H_h \;\rightarrow\; VI \leq K_{VI}, \tag{4.72}$$

$$H_{nh} \;\rightarrow\; VI > K_{VI} \tag{4.73}$$

where $H_h$ is homogenous clutter hypothesis while $H_{nh}$ is non-homogenous clutter hypothesis.

In order to detect inhomogeneities in the windows due to clutter edges, the mean ratio $MR$ is to be used. The mean ratio statistic is defined as

$$MR = \frac{max(\mu_A, \mu_B)}{min(\mu_A, \mu_B)}. \tag{4.74}$$

The expected value of the MR is unity in a homogeneous environment. However, the expected value of the MR increases when targets, discrete clutter or clutter edges are present in the secondary data. The $MR$ is compared with a threshold $K_{MR}$ to decide if the population means in the leading and lagging window halves are about the same or different using the following hypothesis test:

$$H_h \;\rightarrow\; MR \leq K_{MR} \tag{4.75}$$

$$H_{nh} \;\rightarrow\; MR > K_{MR} \tag{4.76}$$

where $H_h$ is homogenous clutter hypothesis and $H_{nh}$ is non-homogenous clutter hypothesis.

Prior to interference power estimation leading and lagging windows are subject to the VI homogeneity test and mean ratio homogeneity test. If both windows are declared homogeneous by both VI and MR test, power estimation is performed with the complete secondary data set. The first row of Table 4.1 corresponds to the case mentioned. If only one of the windows fail the VI homogeneity test and is declared non-homogeneous, the non-homogeneous window is discarded from the secondary data and

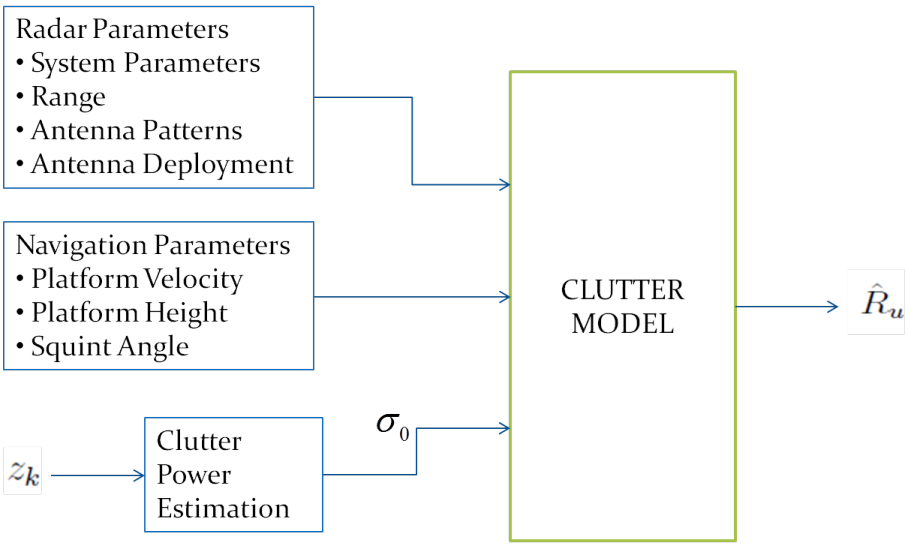


Figure 4.3: Interference Covariance Matrix Generation

estimation is performed with the other window. The second and third rows of Table 4.1 corresponds to that case. If both of the windows are non-homogeneous, interference power estimation is performed with the window which has the smaller interference power. The fourth row of Table 4.1 corresponds to that case. If both windows are declared homogenous by VI but not by the MR test, there is a clutter edge in the guard cells. Therefore the interference power estimation is performed with the window which has the smaller interference power in order to avoid under-estimation which may cause false alarms due to unsuppressed clutter. The output of the interference power estimation is denoted as $\mu$.

Table 4.1: Power Estimation Logic

| $VI_A$Test | $VI_B$Test | $MR$Test | Interference Power Estimation |
|---|---|---|---|
| $H_h$ | $H_h$ | $H_h$ | $\mu = \frac{\mu_A+\mu_B}{2}$ |
| $H_{nh}$ | $H_h$ | - | $\mu = \mu_A$ |
| $H_h$ | $H_{nh}$ | - | $\mu = \mu_B$ |
| $H_{nh}$ | $H_{nh}$ | - | $\mu = min(\mu_A, \mu_B)$ |
| $H_h$ | $H_h$ | $H_{nh}$ | $\mu = max(\mu_A, \mu_B)$ |

The mean clutter radar cross section $\sigma_0$ can be estimated as

$$\widehat{\sigma_0} = -\gamma N \sigma_n^2 + \gamma\mu. \tag{4.77}$$

## 4.5 Model Based GMTI Weighting Vector Calculation

The model for the interference covariance matrix is described in sub-section (1.2). Estimation of the only unknown parameter $\sigma_0$ is explainedin sub-section (1.3). Figure 4.3 shows the block diagram of the estimation procedure of interference covariance matrix. Using the radar and navigational parameters as well as the clutter mean radar cross section estimation,the interference covariance matrix$\hat{R}_u$ is formed. Using this matrix matched filter coefficients will be determined.

The matched filter coefficients can be expressed by

$$W_{MB} = \hat{R}_u^{-1}\mathbf{b} \tag{4.78}$$

where $\mathbf{b}$ is the space-time target steering vector of size $MN$ x 1.

Then, the final form of the detection test statistics becomes

$$l_{MB} = \frac{\left|\mathbf{b}^H \hat{R}_u^{-1}\mathbf{z}\right|^2}{\left|\mathbf{b}^H \hat{R}_u^{-1}\mathbf{b}\right|} \tag{4.79}$$

where $\mathbf{z}$ is the data vector that corresponds to the range bin under test and $\mathbf{z}$ is a vector of size $MN$ x 1 such as

$$\mathbf{z} = \begin{bmatrix} \mathbf{z}(1) \\ \mathbf{z}(2) \\ \vdots \\ \mathbf{z}(N-1) \\ \mathbf{z}(N) \end{bmatrix} \tag{4.80}$$

where $\mathbf{z}(n)$ is a $M$x1 vector and the elements of $\mathbf{z}(n)$ corresponds to the data sampled at each array output for the range bin under test at the pulse $n$.

For the computation of the matched filter coefficients, look up tables that are formed before the operation can be used. Using the estimated clutter power and platform parameters, the appropriate choice of matched filter coefficients can be used. Therefore the only computational load is due to clutter power estimation process. Since the intelligent power estimation method outperforms other methods, it will be used. The computational load required to find the inner-products is $KN$ flops. Variability index calculation requires $K$ flops. The operational counts for intelligent power estimation is

$$IntCFAR_{flop} = O(KN + K). \tag{4.81}$$

# CHAPTER 5

# SIMULATION AND FLIGHT TEST RESULTS

## 5.1 Simulator Data Generation

In order to test the performance of the space time auto-regressive clutter suppression and model-based GMTI, a GMTI simulator was developed. Mentioned clutter suppression techniques are tested under controlled radar parameters for different clutter distributions. SMI Pre-Doppler STAP is also tested for comparison purposes. The radar parameters and antenna patterns can be set as required and different clutter distributions can be chosen for simulations. The available clutter types are :

- Gaussian clutter with desired mean radar cross section
- K-distributed clutter with desired shape parameter and mean radar cross section
- Clutter map (SAR image) based clutter generation

Interference data generation is performed by calculating the covariance of the interference and generating data that has the same interference covariance characteristics. Simulation is performed following the steps described below for each range bin to be simulated:

1. Clutter covariance matrix $R_u$ is generated using equation (4.37).
2. Clutter covariance matrix is decomposed into its eigenvectors and eigenvalues so that
$$R_u = V_u^H D_u V_u. \tag{5.1}$$
3. A vector $\mathbf{x}$ of length $2MN$ with unity variance white Gaussian noise is generated.
$$\mathbf{x} = \mathcal{N}(0, 1). \tag{5.2}$$
4. Clutter simulation data $\mathbf{z}_u$ is obtained by the following operation
$$\mathbf{z}_u = V_u^H D_u^{1/2} \mathbf{x} \tag{5.3}$$
such that covariance of the generated data is
$$R_z = E\left\{\mathbf{z_u z_u}^H\right\} = V_u^H D_u^{1/2} E\left\{\mathbf{x x}^H\right\} D_u^{1/2} V_u = V_u^H D_u V_u = R_u. \tag{5.4}$$
5. The simulation is performed for $2N$ pulses in a CPI; however, only mid-half of the data are used in the simulations to ensure that (5.4) holds .
6. White complex Gaussian noise is added for thermal noise simulation. The variance of noise added is the system noise power.

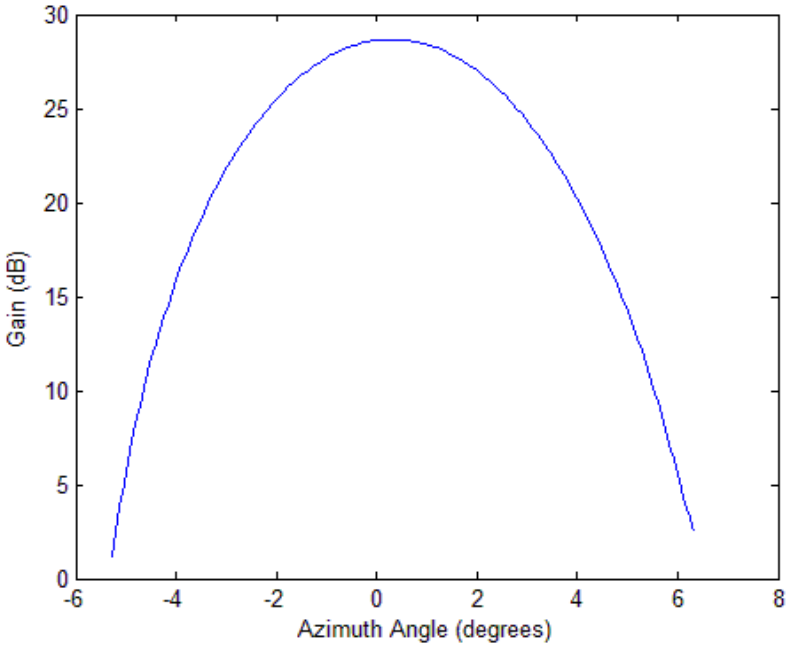


Figure 5.1: Sum Channel Antenna Pattern

Table 5.1: Simulation Radar Parameters

| Parameter | Value |
|---|---|
| Antenna Type | $\Sigma - \Delta$ |
| Platform Height | 2000 m |
| Pulses in CPI ($N$) | 64 |
| Pulse Repetition Frequency | 4000 Hz |
| Platform Velocity | 65 m/s |
| Range Resolution | 6 m |
| Mean Clutter RCS | -20 dBm |
| Noise Figure | 3 dB |
| Pulse Compression Gain | 23 dB |
| Squint Angle | $0^0$ |
| Range | 15 km |

Radar parameters used in simulations are shown in Table (5.1). Antenna patterns used for simulation can be observed in Figure 5.1 and Figure 5.2.

Clutter distribution $\sigma_c^2(x, y)$ used in the first stage of the clutter generation is constant for Gaussian clutter. For SAR image based clutter generation, SAR images are fed into the simulator so that the resulting clutter data have the same covariance as desired. For K-distributed clutter, $\sigma_c^2(x, y)$ is obtained by the product of $\Gamma(\vartheta + 1, 1)$ and $\Gamma(1, 1)$, where $\vartheta$ is the shape parameter and $\Gamma$ is the gamma

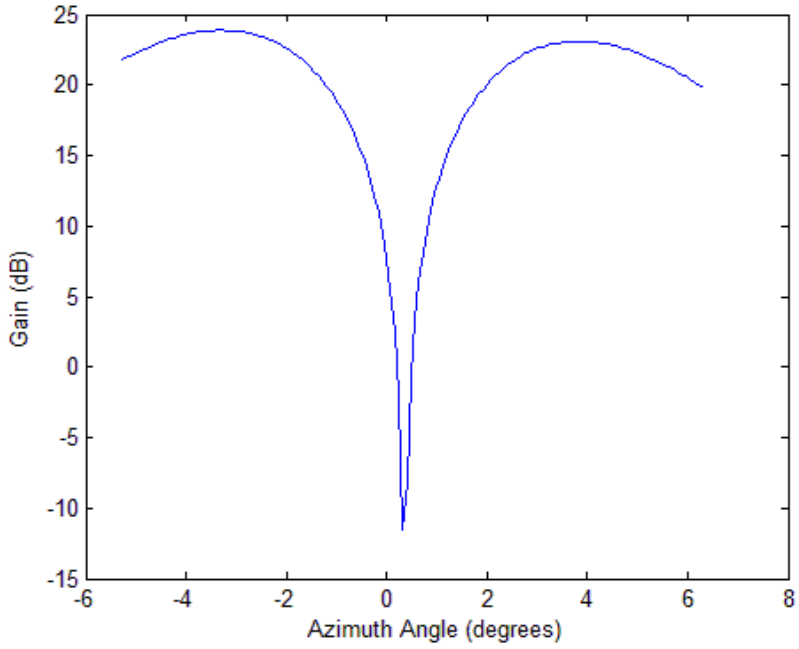


Figure 5.2: Difference Channel Antenna Pattern

distribution symbol. The shape parameter used for simulations is 0.5. The K-distributed clutter map is scaled to the desired mean radar cross section. For each clutter distribution, data generation is repeated 100 times. For the K-distributed clutter case, clutter map generation is repeated for each CPI simulation.

Clutter map based clutter simulation is carried out by two different SAR images. SAR images were obtained by the experimental SAR system developed by ASELSAN. First SAR image corresponds to an area that is relatively flat and the second image corresponds to an area with hills. SAR images that are used in the simulations can be seen in figure (5.3) and figure (5.4).

## 5.2 Flight Test Data

Flight test data were obtained by an experimental SAR system whose parameters are shown in Table 5.2. Data used for analysis are composed of 64 coherent processing intervals. During the test flights, a moving vehicle was deployed in the illuminated area. Radial velocity of the moving vehicle was controlled such that the Doppler of the target would fall in the endoclutter region. Range lines used for the analysis are chosen around the moving target. Total number of range lines used for the analysis are 128. In figure 5.5, Doppler spectrum of a sample coherent processing interval can be observed. In figure 5.5, the target which falls in the 72th Doppler bin and 65th range line is not distinguishable. Actual position of the target is marked with a yellow circle. Since the target is buried under clutter return, it is not distinguishable.

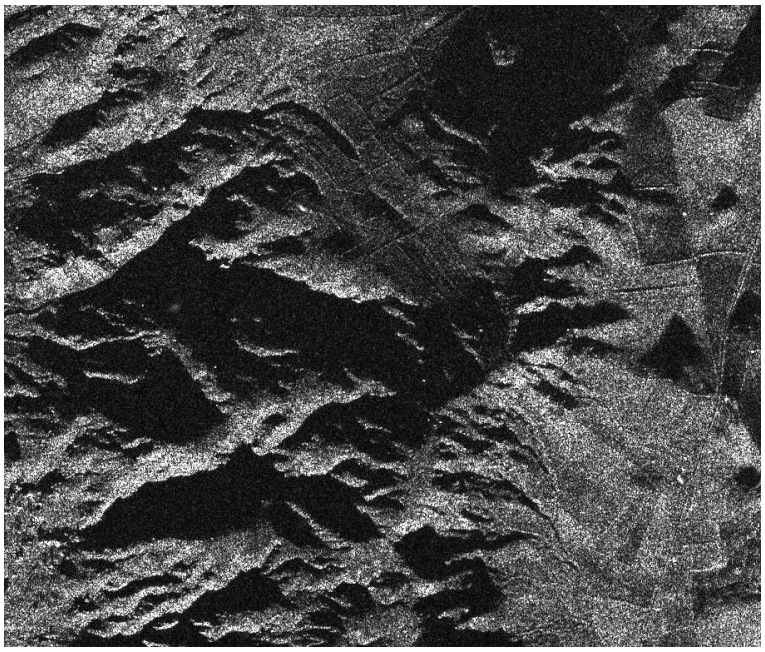

Figure 5.3: Hilly Area SAR Image

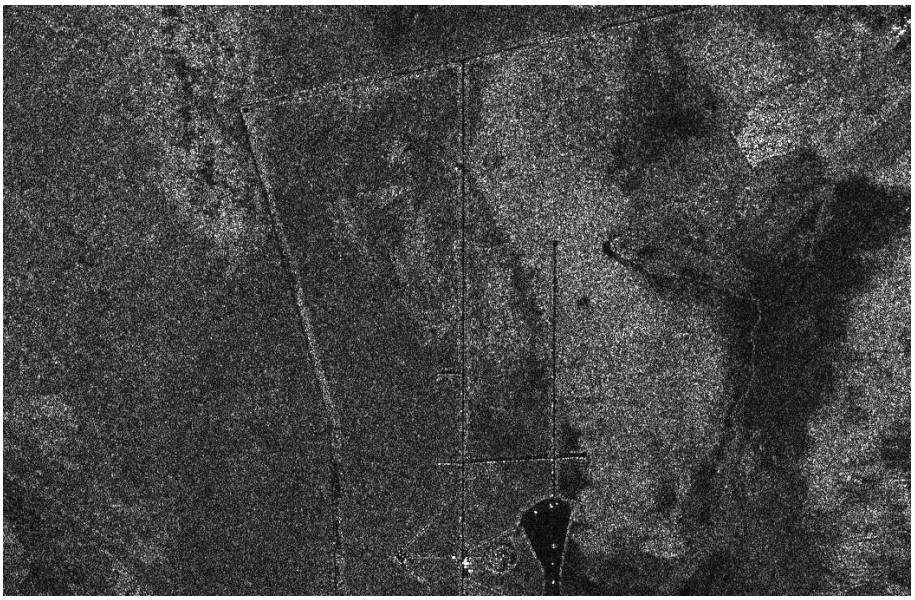

Figure 5.4: Flat Area SAR Image

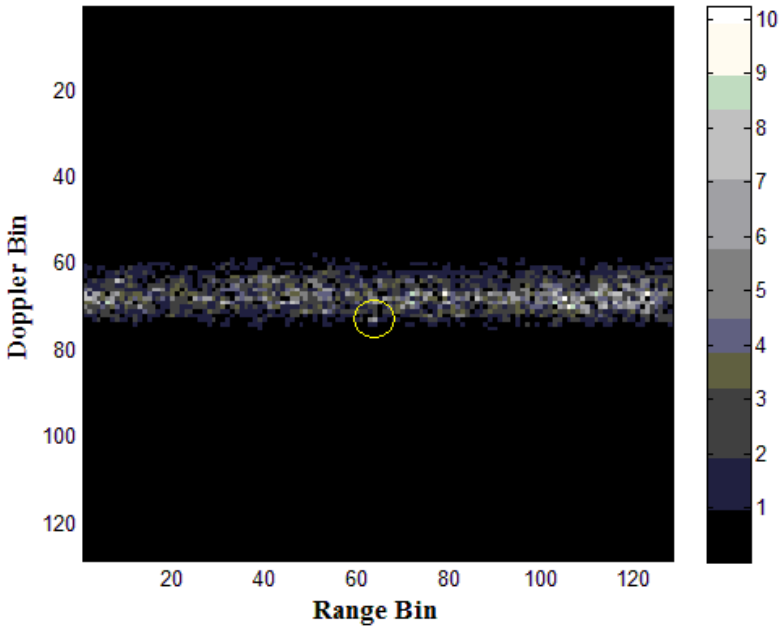


Figure 5.5: Flight Test Data - Sample Range Doppler (The target is the dot enclosed by the circle.) Matrix

## 5.3 STAR Simulation and Flight Test Results

### 5.3.1 STAR Model Order Selection Analysis

In section 3.3 model order estimation was introduced for space-time auto-regressive filtering. In this subsection, model order selection analysis for AIC and MDL criterion are to be investigated using both simulated Gaussian clutter and flight test data obtained during flight tests of the experimental SAR system.

Table 5.2: Flight Test Radar Parameters

| Radar Parameter | Value |
|---|---|
| Platform Height | 2000 m |
| Pulses in CPI ($N$) | 128 |
| Pulse Repetition Frequency | 4000 Hz |
| Platform Velocity | 61 m/s |
| Squint Angle | $\sim 1^0$ -$\sim 5^0$ |
| Range | 14 km |

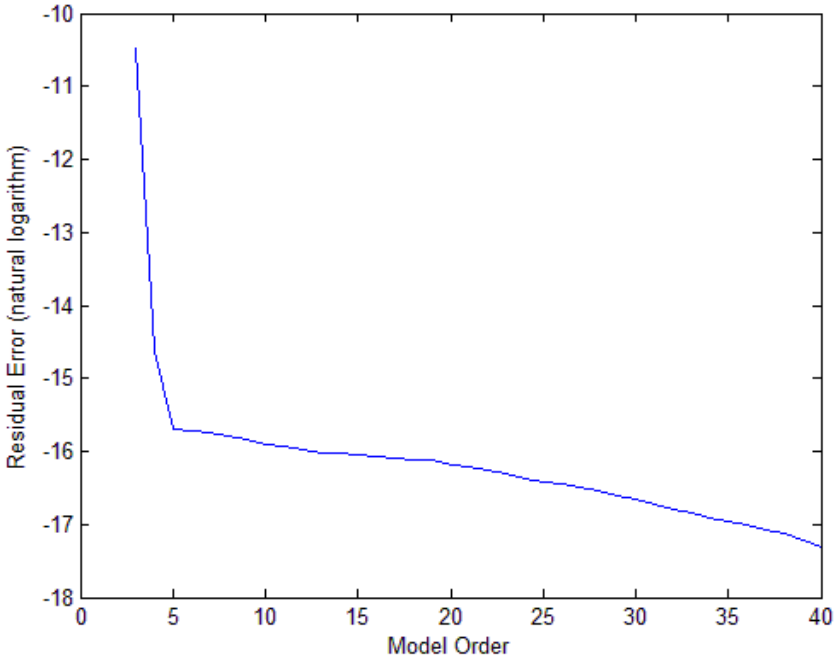


Figure 5.6: Simulation Data Residual Error Determinant - Model Order

#### 5.3.1.1 STAR Model Order Selection for Simulation Data

Data simulated with Gaussian clutter assumption are used in the model order selection si- mulations. In Figure 5.6, the determinant of the residual error matrix is shown for different model orders. The residual error matrix determinant decreases with increasing model order. However after a certain point slope of the residual error changes. For filter order numbers less than 5 there is a sharp change in the determinant, while for filter numbers greater than 5 the decrease is much slower. Since the correlations between pulses decrease as the pulses are separated more in slow time, residual error matrix determinant is expected to decrease less after a certain model order value. Adding the penalty terms for the AIC and MDL criteria, model selection criterion are obtained. The corresponding results are shown in Figure 5.7 and Figure 5.8. Both criterion has a minimum at model order 5. For model orders larger than 5, the decrease in the residual error matrix is less than the increase in the penalty terms. For the simulated data, model order $p = 5$ is chosen as the autoregressive model order. In the model order analysis, the number of singular vectors used to obtain filter taps is $M' = 2$. This value is obtained using (3.15).

#### 5.3.1.2 STAR Model Order Selection for Flight Test Data

In order to perform STAR filtering using the experimental SAR system data, model order selection is performed. In Figure 5.9, the determinant of the residual error matrix is shown for different model orders. The residual error matrix determinant decreases with increasing model order. However after a certain point slope of the decrease changes. For filter order numbers less than 8 there is a sharp change in the determinant, while for filter numbers greater than 8 the decrease is much slower. Adding the penalty terms for the AIC and MDL criteria, model selection criterion are obtained. The corresponding results are shown in Figure 5.10 and Figure 5.11. Both criterion has a minimum at model order 8. For the simulated data model order $p = 8$ is chosen as the autoregressive model order. In the model order analysis, the number of singular vectors used to obtain filter taps is $M' = 2$. This value is obtained

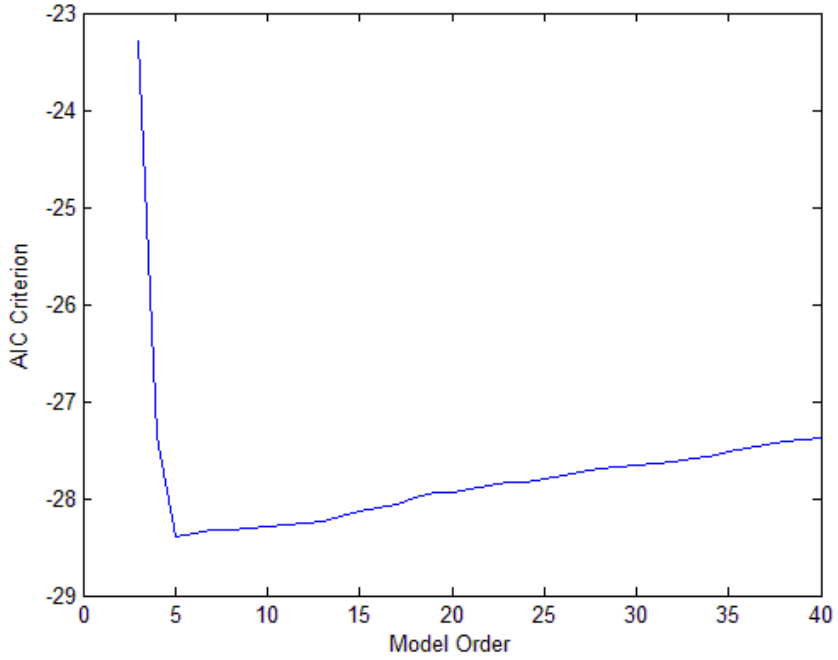


Figure 5.7: Simulation Data AIC Criterion - Model Order (Selected model order is 5)

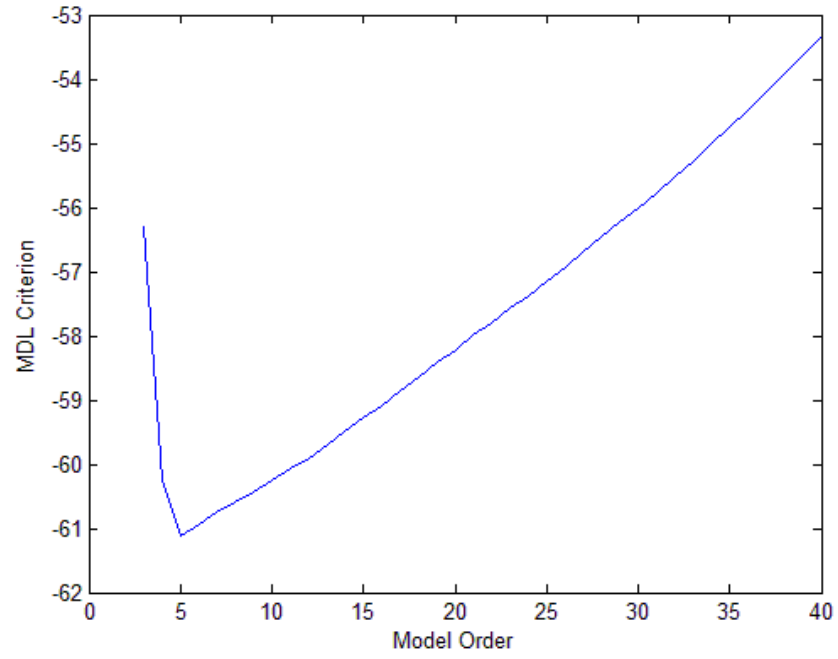


Figure 5.8: Simulation Data MDL Criterion - Model Order (Selected model order is 5)

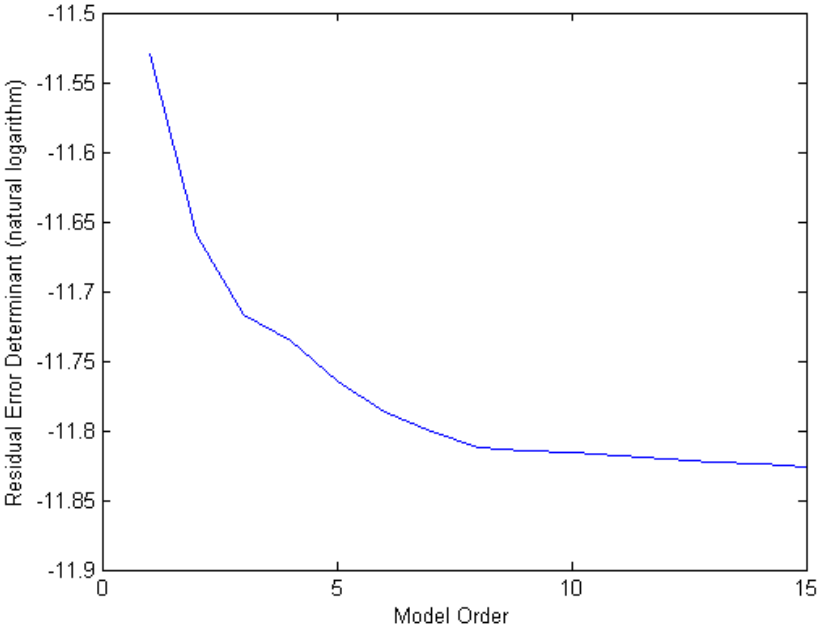


Figure 5.9: Flight Test Data Residual Error Determinant - Model Order

using (3.15).

### 5.3.2 STAR Filtering Performance Analysis

#### 5.3.2.1 STAR Filtering Performance Analysis for Simulation Data

Simulations for STAR filtering are performed for different total secondary range line numbers of $K = 10$ and $K = 40$ in order to test the performance change of STAR filtering with changing secondary data support size. Input and output signal-to-interference ratios for different secondary range lines under different clutter distributions are investigated. Filter order parameters used in the simulations are $p = 5$ and $M' = 2$ for Gaussian clutter. For the K-distributed clutter, filter order parameters and flat area SAR image based clutter are estimated as $p = 7$ and $M' = 2$. For the hilly area SAR image based clutter, filter order parameters are found as $p = 8$ and $M' = 2$. This is due to the fact that clutter rank is higher for these cases resulting in higher correlations for larger set of pulses.

In figures 5.12, 5.13, 5.14, 5.15, 5.16, 5.17, 5.18 and 5.19 input SINR values are shown with red, while the output SINR values are shown in blue. These SINR values are obtained by injecting targets at each Doppler bin separately. For each range bin, the procedure was repeated and the mean SINR values for each range bin is plotted.

Simulation results for SINR analysis of STAR using 10 secondary range lines under Gaussian clutter can be observed in Figure 5.12. Figure 5.13 illustrates the SINR analysis results for K-distributed clutter simulation for STAR filtering using 10 secondary range lines. In Figure 5.14 SINR analysis results for flat area SAR image and in Figure 5.15 SINR analysis results for hilly area SAR image are shown.

Simulation results for for SINR analysis of STAR using 40 secondary range lines can be observed in

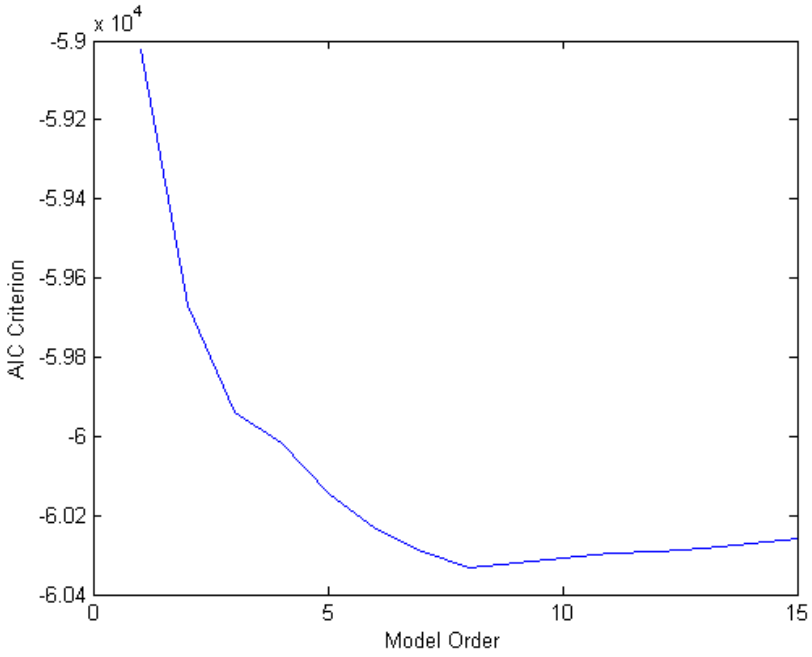


Figure 5.10: Flight Test Data AIC Criterion - Model Order (Selected model order is 8)

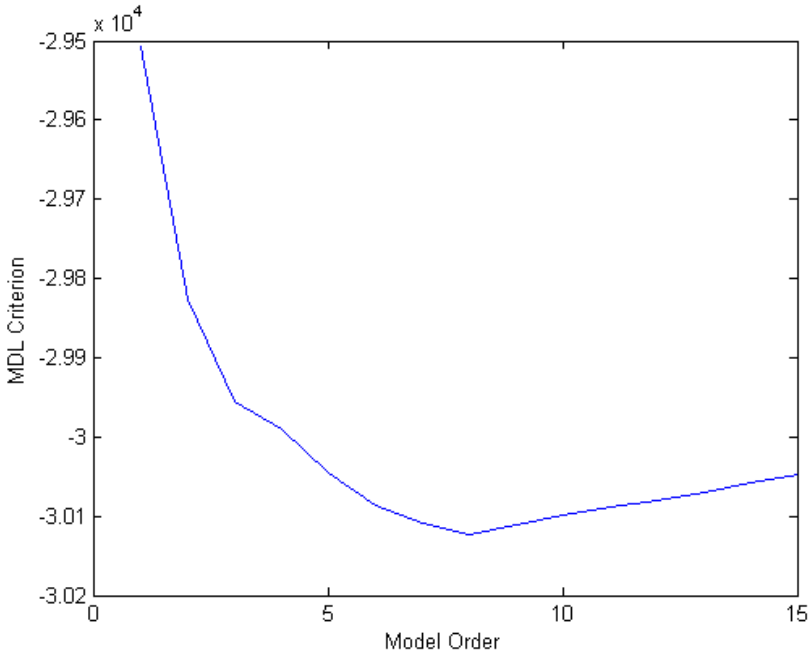


Figure 5.11: Flight Test Data MDL Criterion - Model Order (Selected model order is 8)

Table 5.3: STAR Minimum Detectable Velocity (MDV)

| Clutter Type | MDV | Number of Secondary Range Lines |
|---|---|---|
| Gaussian | 2 m/s | 40 |
| Gaussian | 2.3 m/s | 10 |
| K-Distributed | 2.3 m/s | 40 |
| K-Distributed | 2.8 m/s | 10 |
| Flat Area SAR Image | 2 m/s | 40 |
| Flat Area SAR Image | 2.6 m/s | 10 |
| Hilly Area SAR Image | 2.3 m/s | 40 |
| Hilly Area SAR Image | 2.8 m/s | 10 |

Figure 5.16, Figure 5.17, Figure 5.18 and Figure 5.19 for Gaussian, K-distributed, flat area SAR image based and hilly area SAR image based clutter simulation respectively.

If the SINR required for detection is assumed to be 14 dB, the corresponding minimum detectable velocity values are as shown in Table 5.3. MDV results indicate that STAR filtering can tolerate usage of smaller number of secondary data with some graceful performance degradation. Despite the fact that STAR filtering performs well under different clutter dist- ribution for relatively high secondary sample support, when the secondary sample support is reduced, MDV performance degrades for K-distributed and hilly area SAR image based clutter since inhomogeneities and the clutter rank increases.

#### 5.3.2.2 STAR Filtering Performance Analysis for Flight Test Data

STAR filtering is performed on flight test data for different secondary range line support numbers of $K = 10$ and $K = 40$ in order to test the performance change of STAR filtering with changing secondary data support size. Output signal-to-interference ratios for different secondary range lines under different clutter distributions are investigated. Detection test statistics, that are obtained using STAR filter output, are fed into cell averaging CFAR and resulting detections and false alarms are observed. Filter order parameters estimated from the flight test data are $p = 8$ and $M' = 2$. A sample output for STAR filtering detection test statistics is shown in figure 5.20. CFAR output of the detection test statistics is illustrated in figure 5.21. In figures 5.20 and 5.21, range-Doppler bin corresponding to a controlled moving target is marked with a yellow circle.

Flight test data results for SINR analysis of STAR using 10 secondary range lines can be observed in Figure 5.22 for each CPI. Estimated mean SINR for $K = 10$ secondary range lines, is 25.5 dB. SINR values are estimated using neighbor range bins that have the same Doppler as the target. Similarly, flight test data results for SINR analysis of STAR using 40 secondary range lines are illustrated in Figure 5.22 for each CPI. Estimated mean SINR for $K = 40$ secondary range lines, is 27 dB. Results for $K = 10$ secondary data are shown with blue line while results for $K = 40$ secondary data are shown with red line. Estimated target SINR results indicate that with smaller secondary sample support, SINR output of the STAR filtering decreases. However, the decrease in the performance is not severe.

Figure 5.23 illustrates the CFAR output of the detection test statistics obtained by STAR filtering with $K = 10$ secondary range lines. Similarly Figure 5.24 illustrates the CFAR output of the detection test statistics obtained by STAR filtering with $K = 40$ secondary range lines. For each CPI, detections obtained are marked with small circles on the range-Doppler map according to the range bin and Doppler bin of the detections. Detections for the controlled moving target are marked with a black circle. Cell averaging CFAR is performed for false alarm probability of $10^{-6}$. Since the analysis is performed for 64 CPI, 128 Doppler bins, 96 remaining range bins and false alarm probability of $10^{-6}$, the expected number of false alarms is in the order of 1. However, in figure 5.23 one can observe that

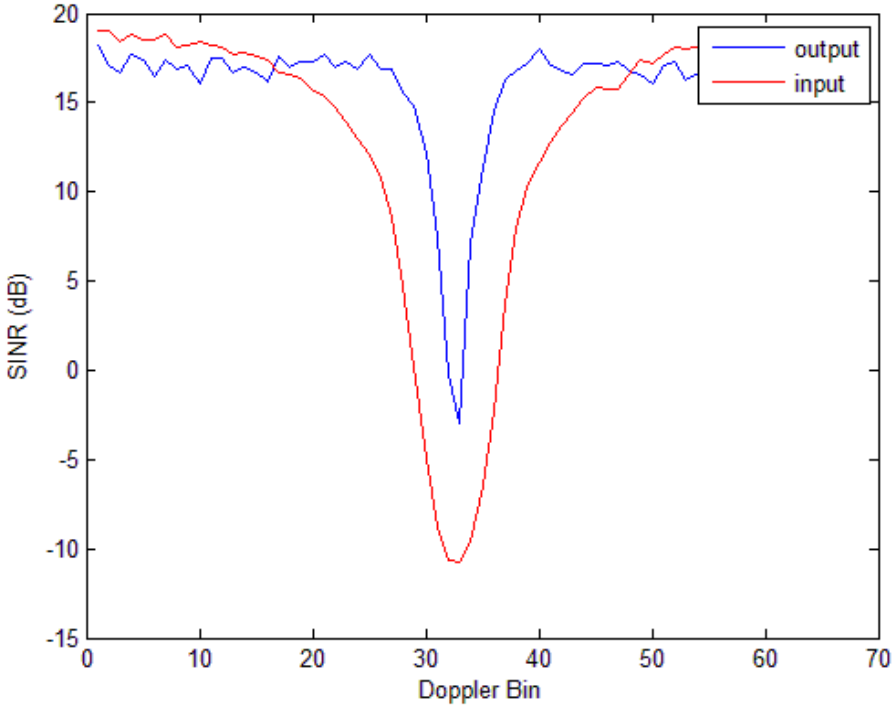


Figure 5.12: STAR SINR Analysis for Gaussian Clutter Simulation with K=10

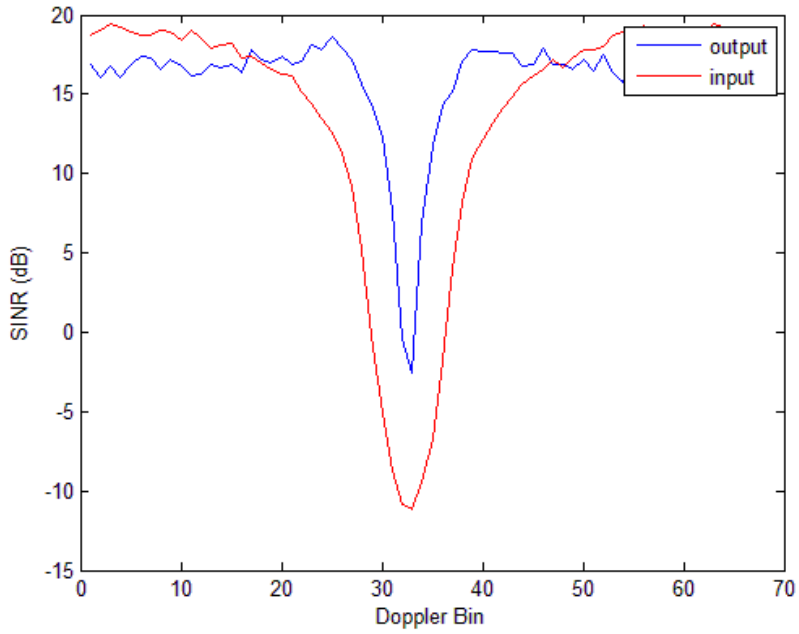


Figure 5.13: STAR SINR Analysis for K-Distributed Clutter Simulation with K=10

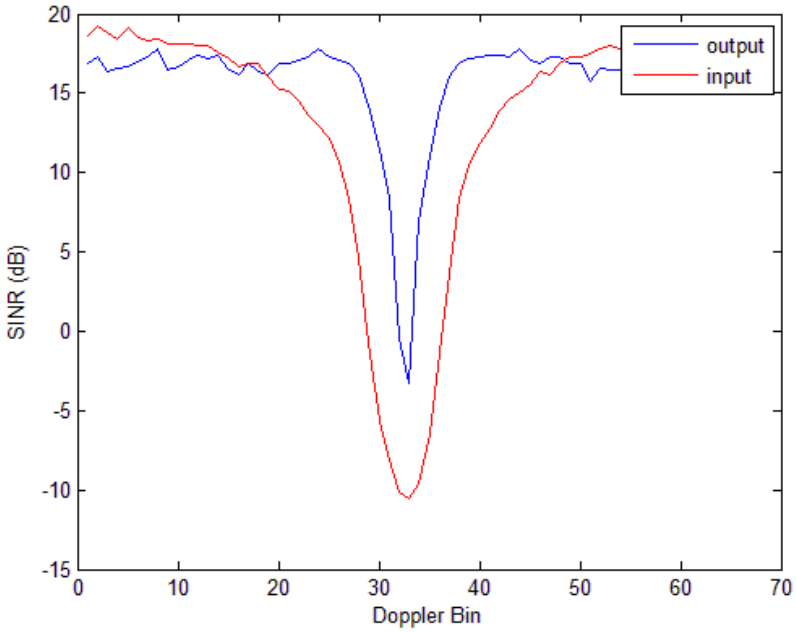


Figure 5.14: STAR SINR Analysis for Clutter Simulation based on Flat Area SAR Image with K=10

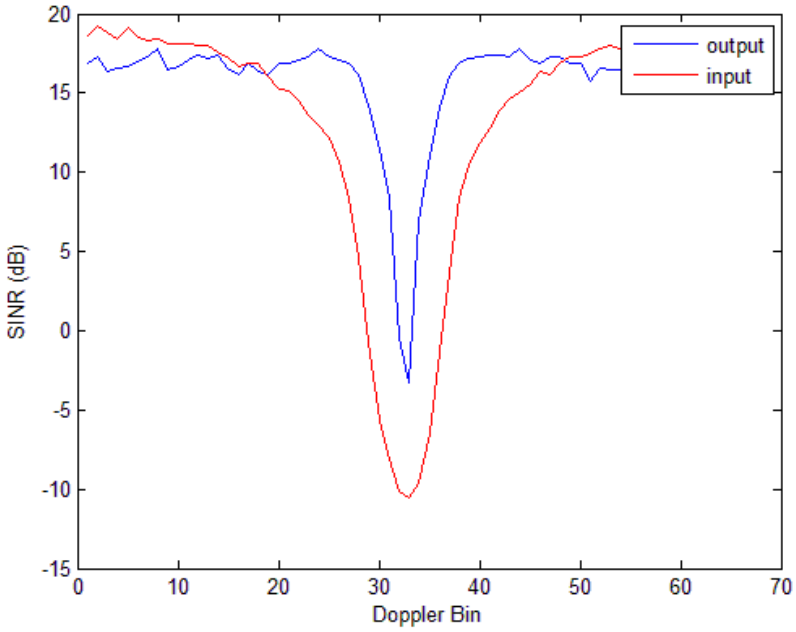


Figure 5.15: STAR SINR Analysis for Clutter Simulation based on Hilly Area SAR Image with K=10

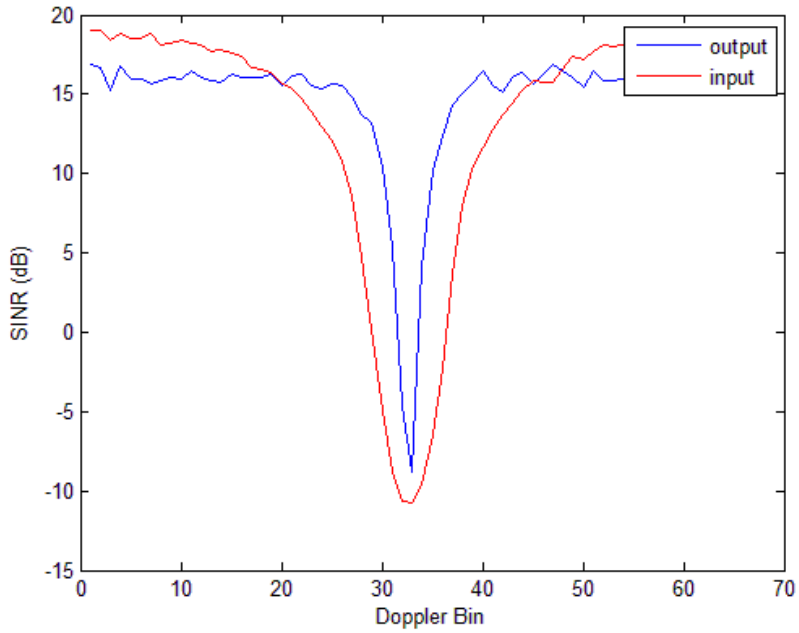


Figure 5.16: STAR SINR Analysis for Gaussian Clutter Simulation with K=40

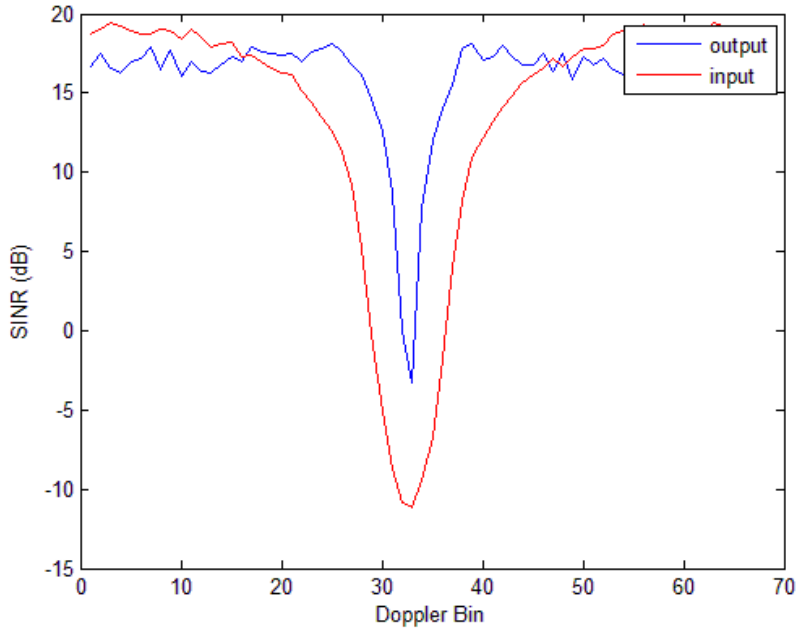


Figure 5.17: STAR SINR Analysis for K-Distributed Clutter Simulation with K=40

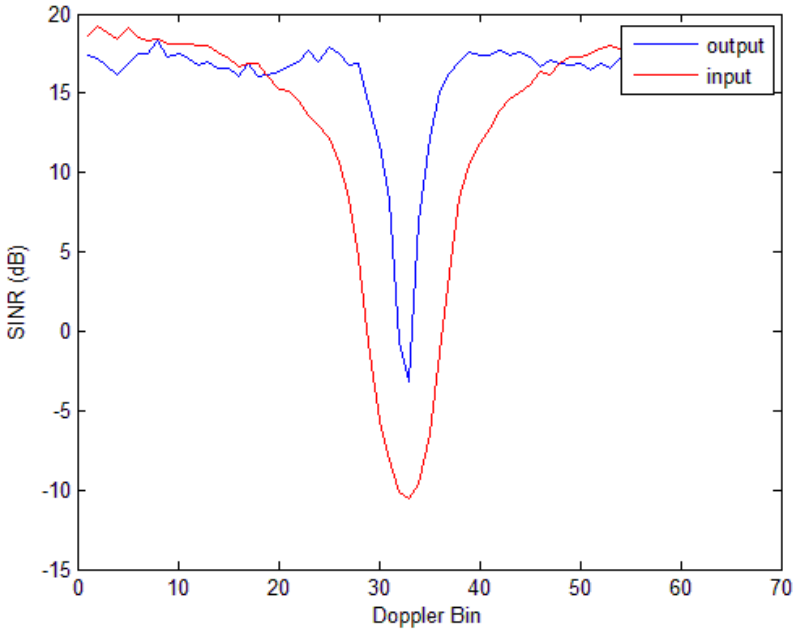


Figure 5.18: STAR SINR Analysis for Clutter Simulation based on Flat Area SAR Image with K=40

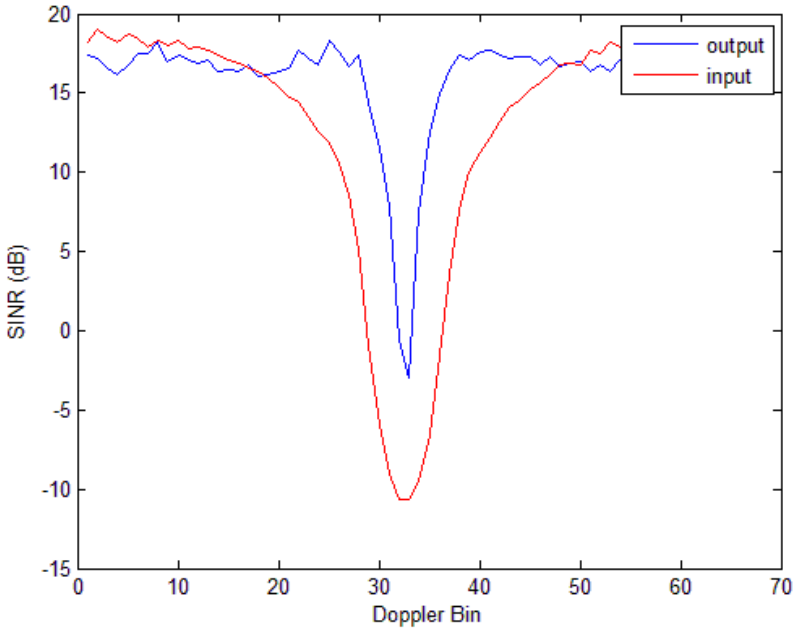


Figure 5.19: STAR SINR Analysis for Clutter Simulation based on Hilly Area SAR Image with K=40

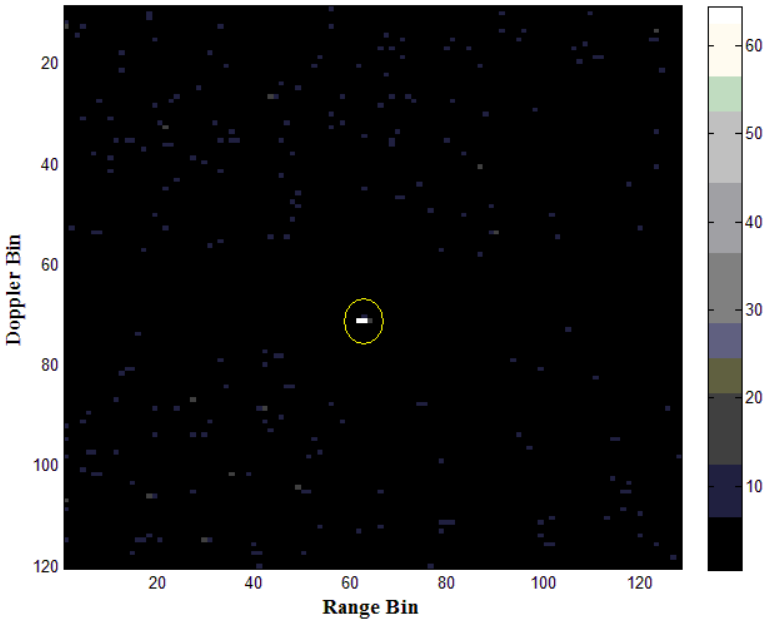


Figure 5.20: STAR Filtering Flight Test Data Sample Detection Test Statistics (The target is the dot enclosed by the circle.)

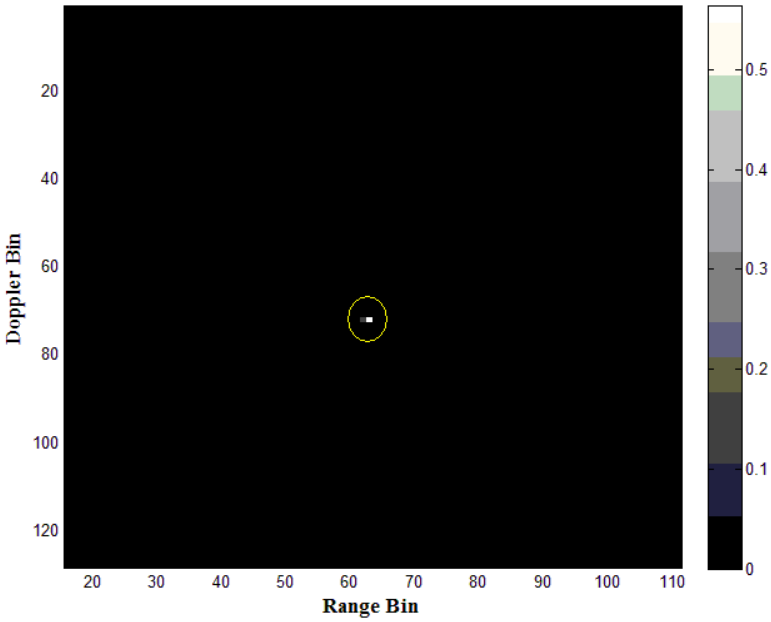


Figure 5.21: STAR Filtering Flight Test Data Sample Detection Test Statistics CFAR Output (The target is the dot enclosed by the circle.)

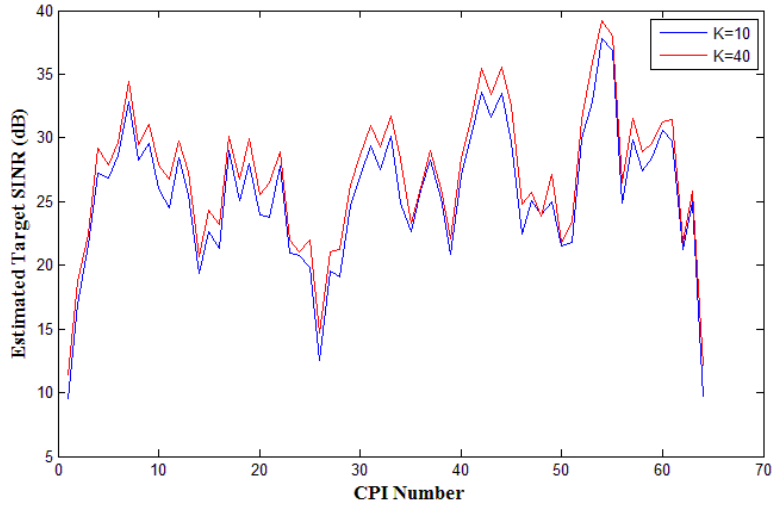


Figure 5.22: STAR Filtering Flight Test Data SINR Analysis

number of false alarms is much larger than the expected value. This is due to the fact that the detection test statistics has lost its Gaussian property. Detection test statistics are not Gaussian distributed and much more spiky than expected. Investigating the results shown in figure 5.24, it can be stated that with increasing secondary range lines ($K = 40$ ), detection test statistics become less spiky and the number of false alarms decreases. Despite the fact that SINR loss with smaller secondary range data is graceful, the CFAR property of the detection test statistics for STAR filtering is heavily dependent on secondary sample data.

## 5.4 Model based GMTI Simulation and Flight Test Results

### 5.4.1 Clutter Power Estimation Performance Analysis

#### 5.4.1.1 Clutter Edge Effects on Clutter Power Estimation Techniques

In order to test the power estimation methods proposed, a clutter edge is simulated. In the simulations the number of range bins is 140. For the first 70 range lines the mean clutter radar cross section value is -35 dB, while for the remaining range lines the value is 0 dB. Each of the algorithms use 20 secondary range lines to estimate the clutter power. The guard range lines around the test lines are chosen as 2 for each window. In figure 5.25, performance of the clutter power estimators can be observed. The color codes of the different estimation techniques are given as legends on the figure. As it can be seen from the figure, simple estimation starts over estimating the clutter power as the edge moves in the secondary data window. After the edge the simple estimation procedure underestimates the clutter power. The IP-NHD (Inner Product Non-Homogeneity Detector) estimator compensates the edge for a couple of range bins more since it eliminates the range lines that has large clutter power. However as the number of range bins that have larger clutter power, IP-NHD does not treat those range bins as outliers and starts working similar to simple power estimation. The intelligent estimation technique, estimates the clutter power accurately for most of the range bins. However for the range bins where the clutter edge is in the guard cells, the intelligent estimation technique overestimates the clutter power. Simulation results show that the intelligent estimation is superior to the other estimation techniques considering the inhomogeneities due to clutter edge.

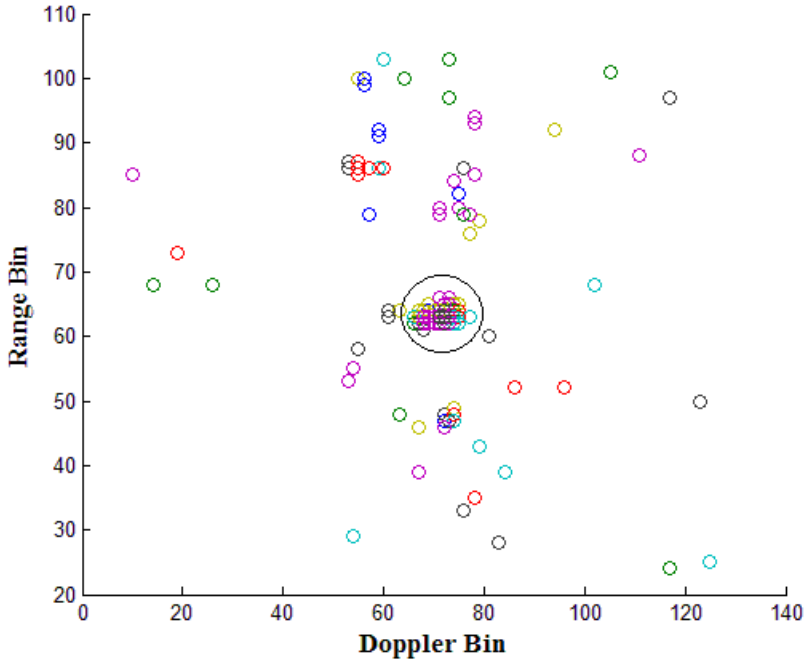


Figure 5.23: STAR Filtering Flight Test Data Detection Test Statistics CFAR Detections for $K = 10$ (Detections due to the target are enclosed by the circle.)

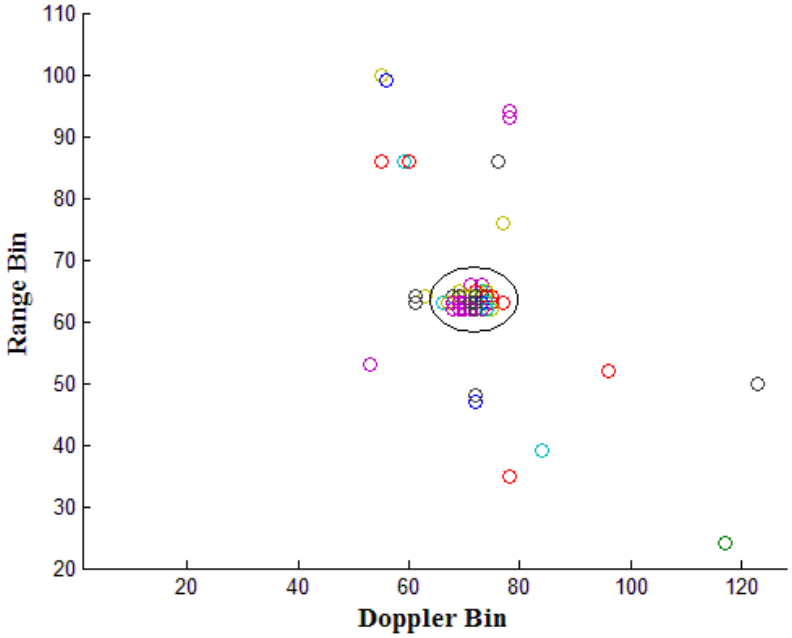


Figure 5.24: STAR Filtering Flight Test Data Detection Test Statistics CFAR Detections for $K = 40$ (Detections due to the target are enclosed by the circle.)

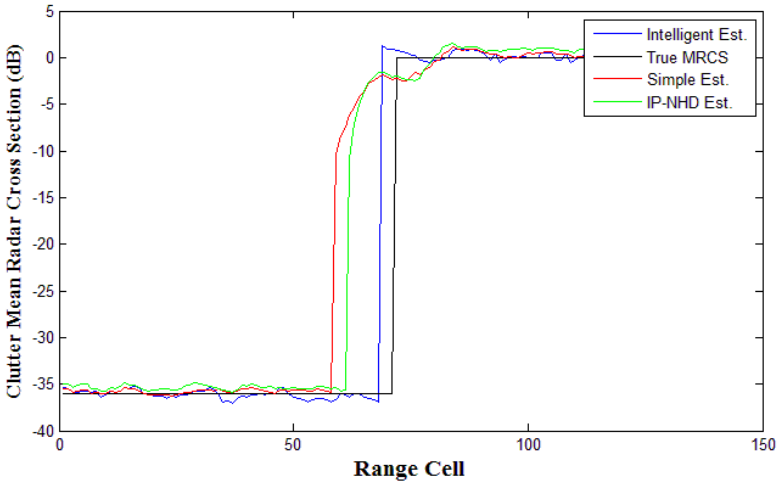


Figure 5.25: Clutter Edge - Clutter Mean RCS Estimation

#### 5.4.1.2 Target in the Secondary Data Effects on Clutter Power Estimation Techniques

In order to test the proposed power estimation methods, a target at range line 70 is simulated. In the simulations the number of range bins is 140. The signal to clutter ratio of the target is 20 dB at the input of the estimator. Each of the algorithms use 20 secondary range lines to estimate the clutter power. The guard range lines around the test lines are chosen as 2 for each window. In figure 5.26, performance of the clutter power estimators can be observed. The color codes of the different estimation techniques are given as legends on the figure. As it can be seen from the figure, simple estimation starts over estimating the clutter power as the target falls in the secondary data window. The IP-NHD (Inner Product Non-Homogeneity Detector) estimator compensates the target effect since it eliminates the range line that contains the target. The intelligent estimation technique, estimates the clutter power accurately since it eliminates the window containing the target. However the estimation of the clutter power varies more than IP-NHD since it uses half of the secondary data for estimation. Simulation results show that both IP-NHD and the intelligent estimation methods eliminate the target during power estimation. However since IP-NHD is able to use more secondary data, it estimates the clutter power more accurately.

### 5.4.2 Model Based GMTI Performance Analysis

#### 5.4.2.1 Model Based GMTI Performance Analysis for Simulation Data

Simulations for Model-based GMTI are performed for secondary range lines of $K = 20$ for clutter power estimation. Input and output signal-to-interference ratios under different clutter distributions are investigated. Clutter power estimation is performed using the intelligent clutter power estimation technique, since it outperforms simple clutter power estimation and IP-NHD power estimator.

Simulation results for SINR analysis of model based GMTI using 20 secondary range bins to estimate the clutter power can be observed in figures 5.27, 5.28, 5.29 and 5.30 for Gaussian, K-distributed, flat area SAR image based and hilly area SAR image based clutter simulation, respectively. In figures 5.27, 5.28, 5.29 and 5.30 input SINR values are shown with red, while the output SINR values are shown in blue. These SINR values are obtained by injecting targets at each Doppler bin separately. For each range bin, the procedure was repeated and the mean SINR values for each range bin is

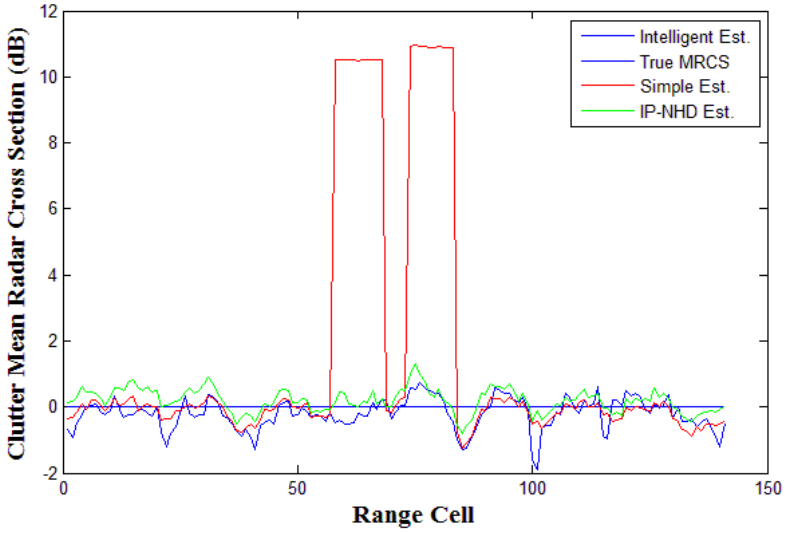


Figure 5.26: Target in Secondary Data - Clutter Mean RCS Estimation

Table 5.4: Model Based GMTI Minimum Detectable Velocity (MDV)

| Clutter Type | MDV |
|---|---|
| Gaussian | - |
| K-Distributed | 3 m/s |
| Flat Area SAR Image | 2.5 m/s |
| Hilly Area SAR Image | 3.5 m/s |

plotted. When the SINR required for detection is assumed to be 14 dB, the corresponding minimum detectable velocity values are as shown in Table 5.4. Since the model-based GMTI and the GMTI simulator uses the same clutter covariance model, minimum detectable velocity for Gaussian clutter is omitted. Model-based GMTI clutter model was built on the assumption that the clutter is Gaussian distributed. The clutter power estimation is also performed for range lines which requires that the clutter distribution in a single iso-range line is homogeneous. However for the hilly area SAR image based clutter generation and K-Distributed clutter generation, that is not the case. Therefore, in the Doppler bins that corresponds to inhomogeneities in the iso-range line, SINR is decreased which results in larger MDV values.

#### 5.4.2.2 Model Based GMTI Performance Analysis for Flight Test Data

Model based GMTI is performed on flight test data for clutter power estimation secondary range line support number of $K = 20$ in order to test the performance change of model based GMTI. Output signal-to-interference plus noise ratios are investigated. Detection test statistics, that are obtained using model based GMTI output, are fed into cell averaging CFAR and resulting detections and false alarms are observed. A sample output for model based GMTI detection test statistics is shown in figure 5.31. CFAR output of the detection test statistics is illustrated in figure 5.32. In figures 5.31 and 5.32, range-Doppler bin corresponding to controlled moving target is marked with a yellow circle.

Flight test data results for SINR analysis of model based GMTI using 20 secondary range lines for

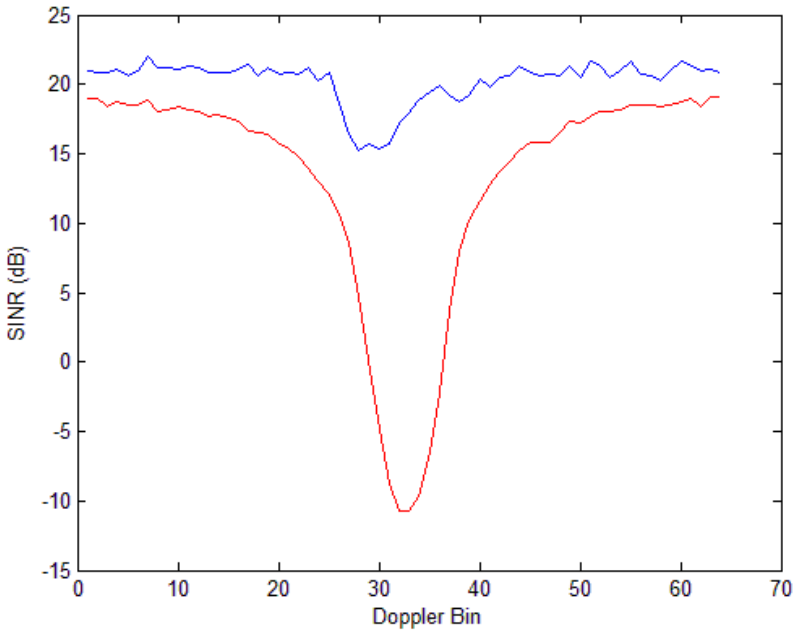


Figure 5.27: Model Based GMTI SINR Analysis for Gaussian Clutter Simulation

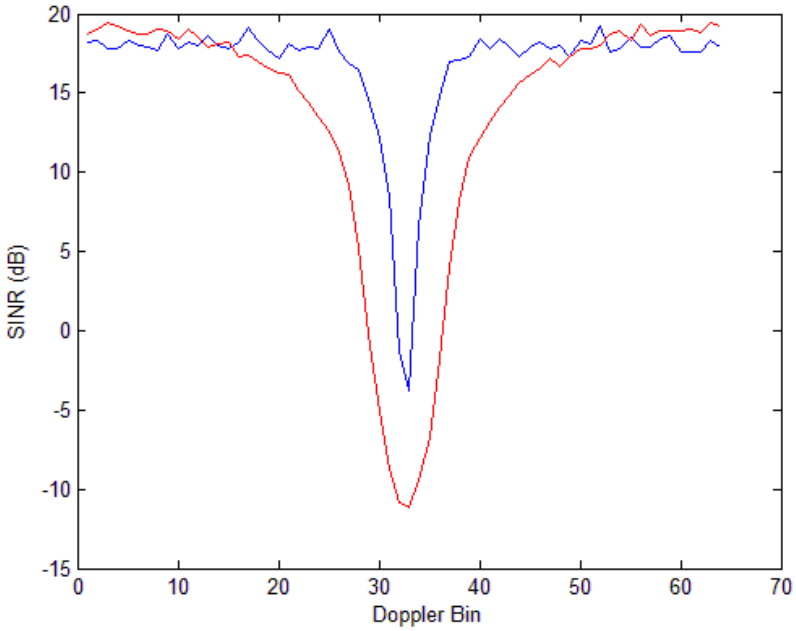


Figure 5.28: Model Based GMTI SINR Analysis for K-Distributed Clutter Simulation

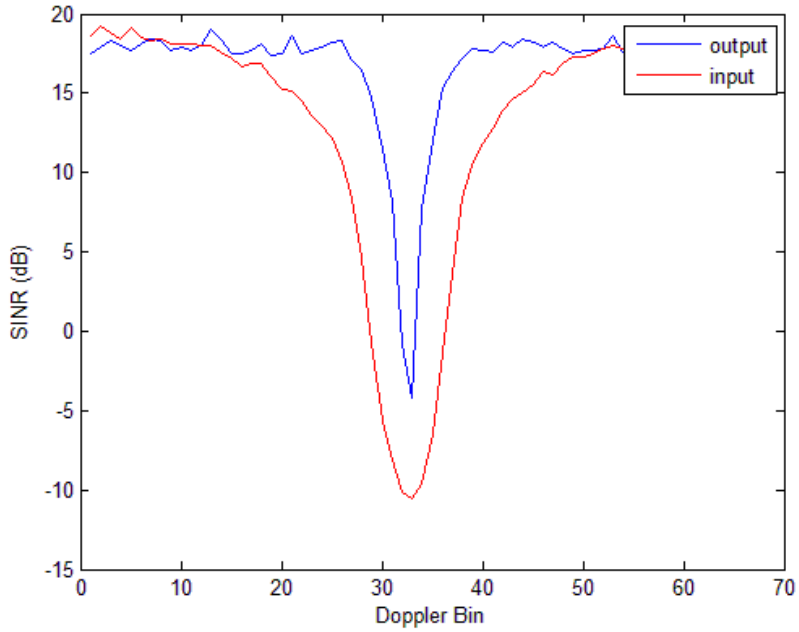


Figure 5.29: Model Based GMTI SINR Analysis for Clutter Simulation based on Flat Area SAR Image

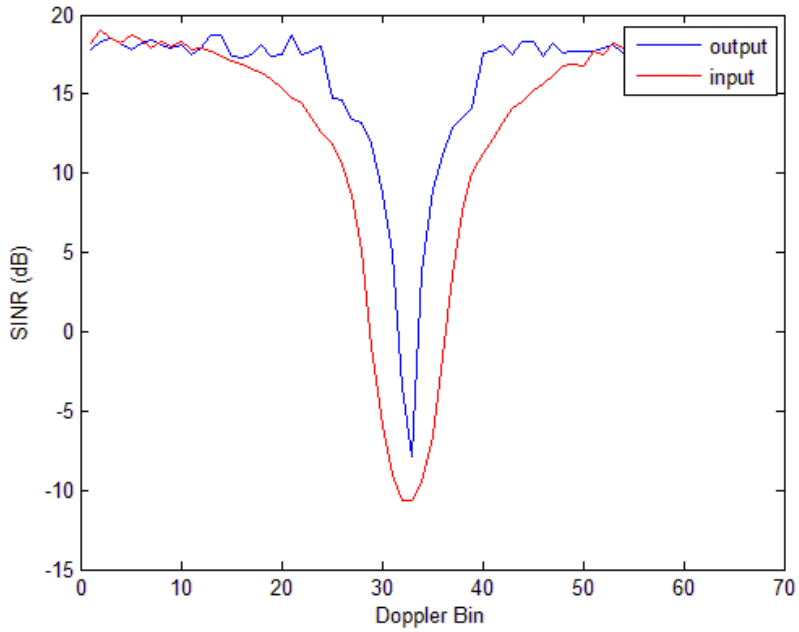


Figure 5.30: Model Based GMTI SINR Analysis for Clutter Simulation based on Hilly Area SAR Image

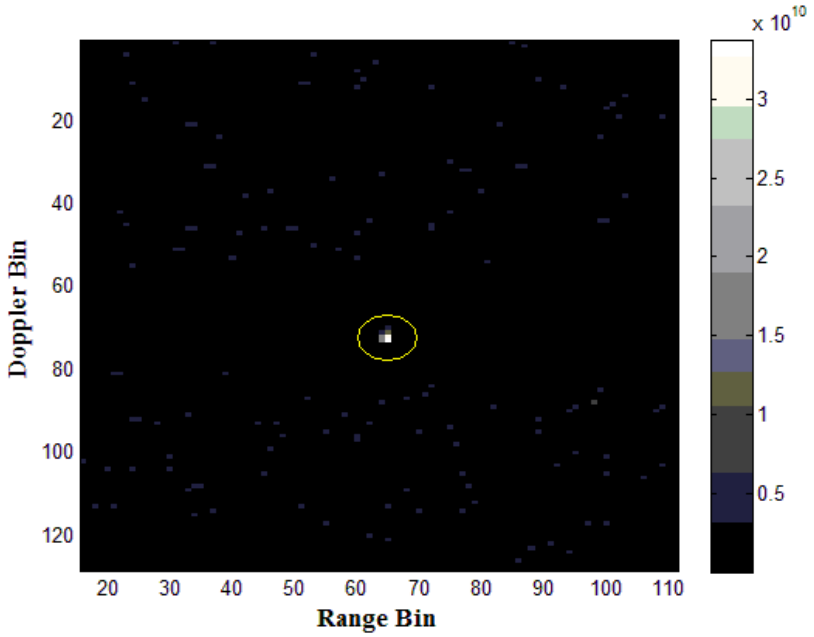


Figure 5.31: Model Based GMTI Flight Test Data Sample Detection Test Statistics (The target is the dot enclosed by the circle.)

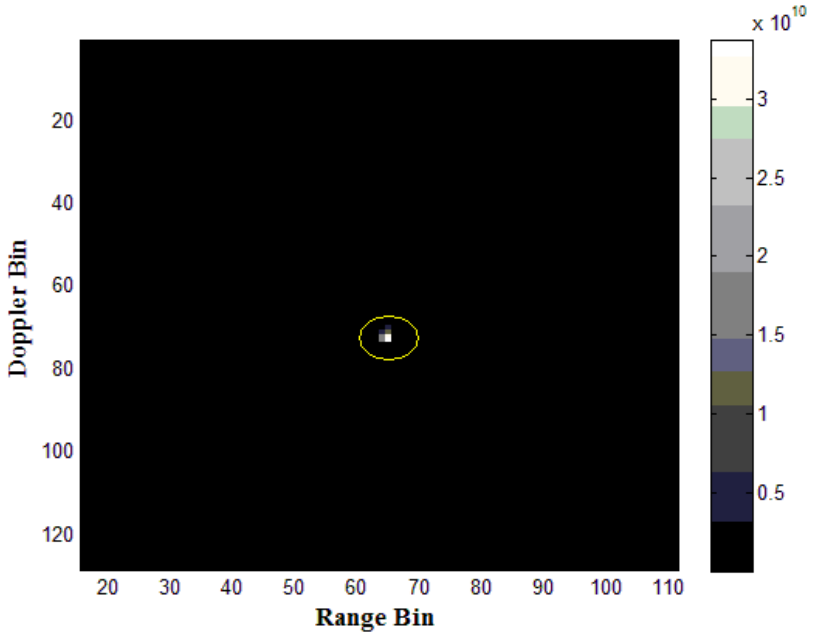


Figure 5.32: Model Based GMTI Flight Test Data Sample Detection Test Statistics CFAR Output (The target is the dot enclosed by the circle.)

clutter power estimation can be observed in Figure 5.33 for each CPI. Estimated mean SINR for $K = 10$ secondary range lines, is 21.5 dB. SINR values are estimated using neighbor range bins that have the same Doppler as the target. Estimated target SINR results indicate that model based GMTI suffers an additional SINR loss which may be a result of internal clutter motion, modeling imperfections and model assumption violations like platform velocity variation.

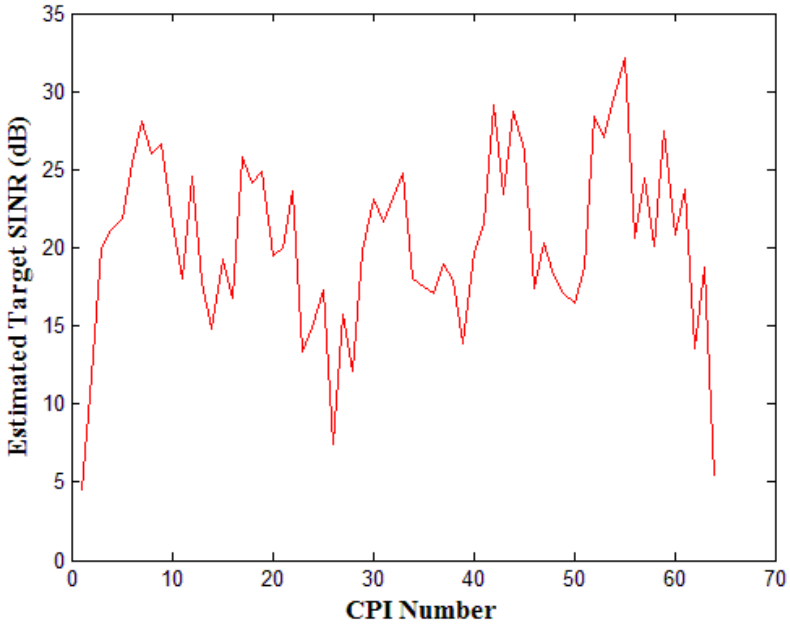


Figure 5.33: Model Based GMTI Flight Test Data SINR Analysis

Figure 5.34 illustrates the CFAR output of the detection test statistics obtained by model based GMTI. For each CPI, detections obtained are marked with small circles on the range-Doppler map according to the range bin and Doppler bin of the detections. Detections for the controlled moving target are marked with a black circle. Cell averaging CFAR is performed for a false alarm probability of $10^{-6}$. Since the analysis is performed for 64 CPI, 128 Doppler bins, 96 remaining range bins and false alarm probability of $10^{-6}$, the expected number of false alarms is in the order of 1. However, in figure 5.34 one can observe that number of false alarms is larger than the expected value. This is due to the fact that the detection test statistics has lost its Gaussian property as a result of the inhomogeneties in the isorange lines.

## 5.5 SMI Pre-Doppler STAP Approach Simulation and Flight Test Results

### 5.5.1 Performance Analysis of SMI Pre-Doppler STAP for Simulation Data

Simulations for SMI Pre-Doppler STAP are performed for different total secondary range line numbers of $K = 10$ and $K = 40$ in order to test the performance change of SMI Pre-Doppler STAP with changing secondary data support size. Input and output signal-to-interference ratios for different secondary range lines under different clutter distributions are investigated.

Simulation results for SINR analysis of SMI Pre-Doppler STAP using 10 secondary range lines under Gaussian clutter can be observed in Figure 5.35. Figure 5.36 illustrates the SINR analysis results for

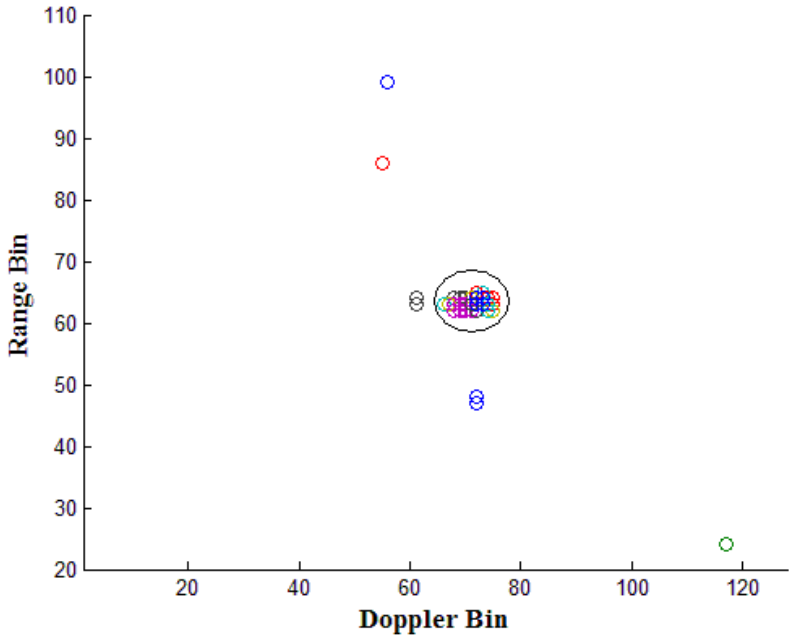


Figure 5.34: Model Based GMTI Flight Test Data Detection Test Statistics CFAR Detections (Detections due to the target are enclosed by the circle.)

K-distributed clutter simulation for SMI Pre-Doppler STAP using 10 secondary range lines. In Figure 5.37 SINR analysis results for flat area SAR image and in Figure 5.38 SINR analysis results for hilly area SAR image are shown.

In the figures 5.35, 5.36, 5.37, 5.38, 5.39, 5.40, 5.41 and 5.42 input SINR values are shown with red, while the output SINR values are shown in blue. These SINR values are obtained by injecting targets at each Doppler bin separately. For each range bin, the procedure was repeated and the mean SINR values for each range bin is plotted.

Simulation results for for SINR analysis of SMI Pre-Doppler STAP using 40 secondary range lines can be observed in Figure 5.39, Figure 5.40, Figure 5.41 and Figure 5.42 for Gaussian, K-distributed, flat area SAR image based and hilly area SAR image based clutter simulation respectively.

If the SINR required for detection is assumed to be 14 dB, the corresponding minimum detectable velocity values are as shown in Table 5.5. MDV results indicate that SMI Pre-Doppler STAP can not tolerate usage of smaller number of secondary data with graceful performance degradation. Since secondary sample data support is not enough to estimate the interference covariance matrix, MDV values for fewer secondary range bins are beyond the endoclutter region. Therefore targets with small radial velocities can not be detected.

### 5.5.2 Performance Analysis of SMI Pre-Doppler STAP for Flight Test Data

SMI Pre-Doppler STAP is performed on flight test data for different secondary range line support numbers of $K = 10$ and $K = 40$ in order to test the performance change of SMI Pre-Doppler STAP with changing secondary data support size. Output signal-to-interference ratios for different secondary range lines under different clutter distributions are investigated. Detection test statistics, that are obtained using SMI Pre-Doppler STAP filter output, are fed into cell averaging CFAR and

Table 5.5: SMI Pre-Doppler STAP Minimum Detectable Velocity (MDV)

| Clutter Type | MDV | Number of Secondary Range Lines |
|---|---|---|
| Gaussian | 3 m/s | 40 |
| Gaussian | 8 m/s | 10 |
| K-Distributed | 3.5 m/s | 40 |
| K-Distributed | 8.5 m/s | 10 |
| Flat Area SAR Image | 3 m/s | 40 |
| Flat Area SAR Image | 8 m/s | 10 |
| Hilly Area SAR Image | 4 m/s | 40 |
| Hilly Area SAR Image | 8.5 m/s | 10 |

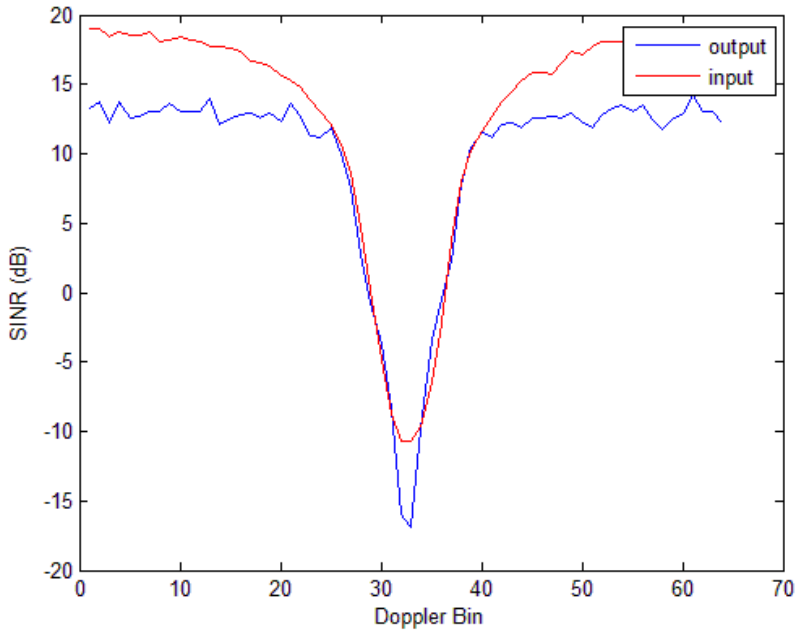


Figure 5.35: SMI Pre-Doppler STAP SINR Analysis for Gaussian Clutter Simulation with K=10

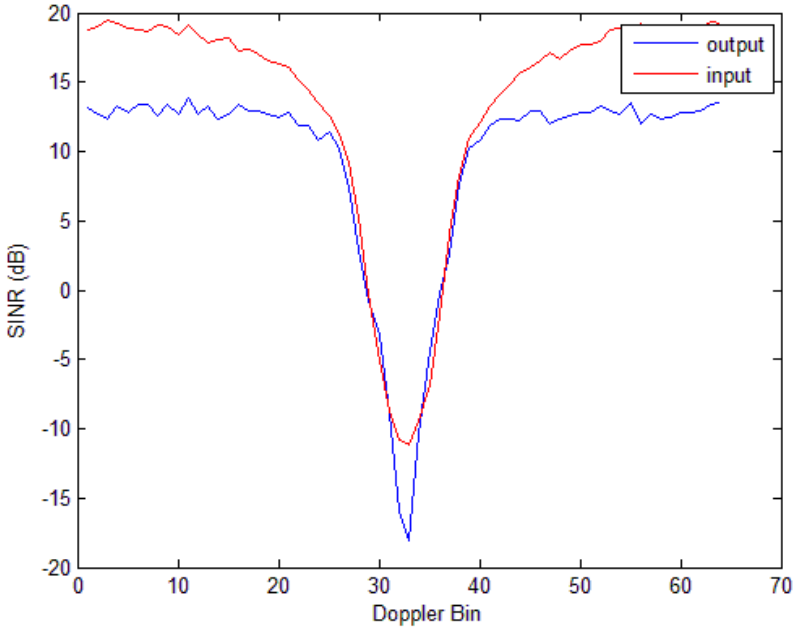


Figure 5.36: SMI Pre-Doppler STAP SINR Analysis for K-Distributed Clutter Simulation with K=10

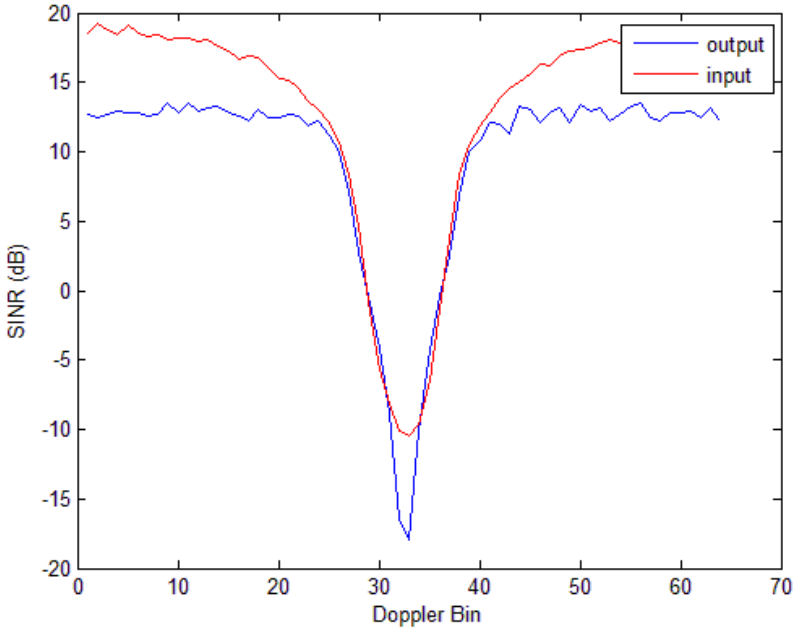


Figure 5.37: SMI Pre-Doppler STAP SINR Analysis for Clutter Simulation based on Flat Area SAR Image with K=10

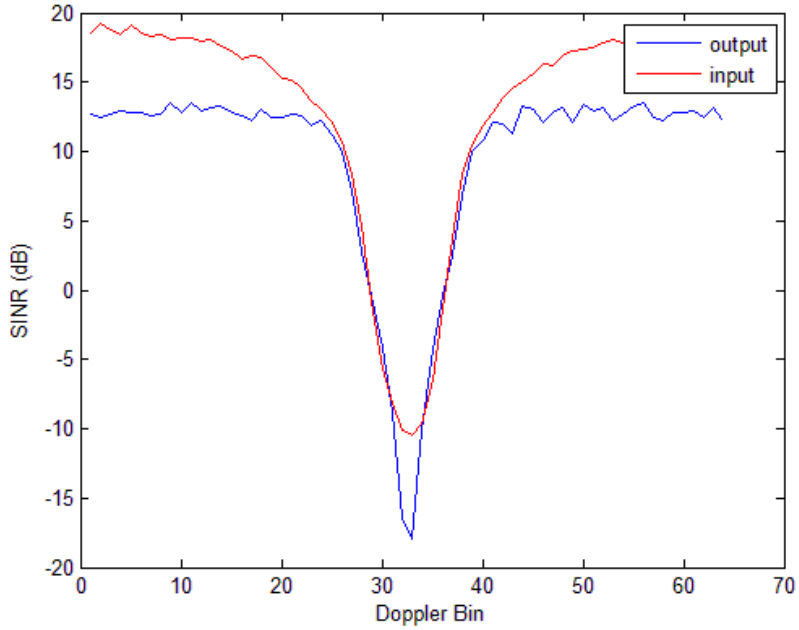


Figure 5.38: SMI Pre-Doppler STAP SINR Analysis for Clutter Simulation based on Hilly Area SAR Image with K=10

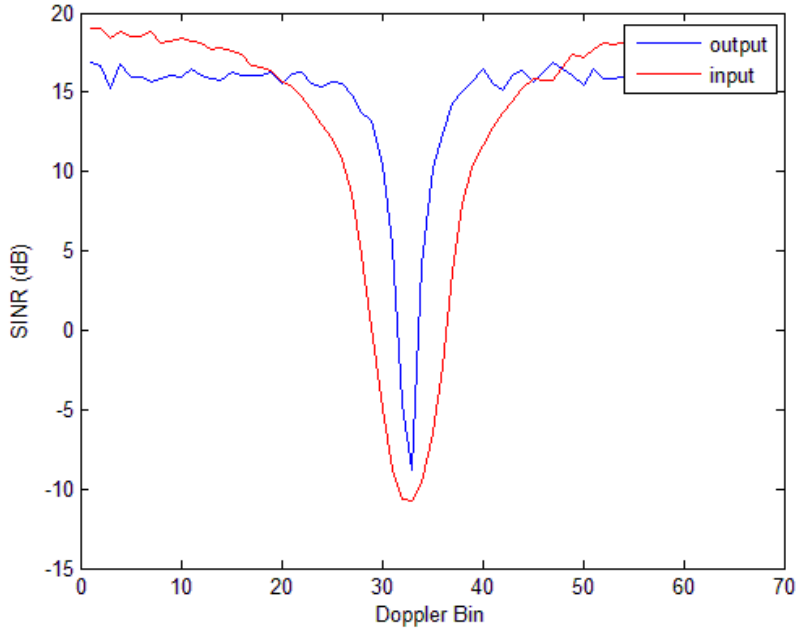


Figure 5.39: SMI Pre-Doppler STAP SINR Analysis for Gaussian Clutter Simulation with K=40

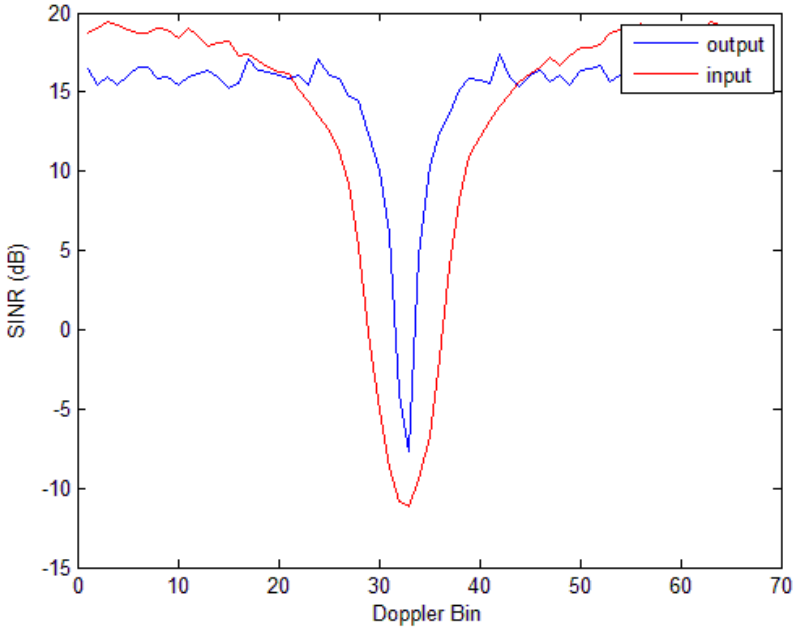


Figure 5.40: SMI Pre-Doppler STAP SINR Analysis for K-Distributed Clutter Simulation with K=40

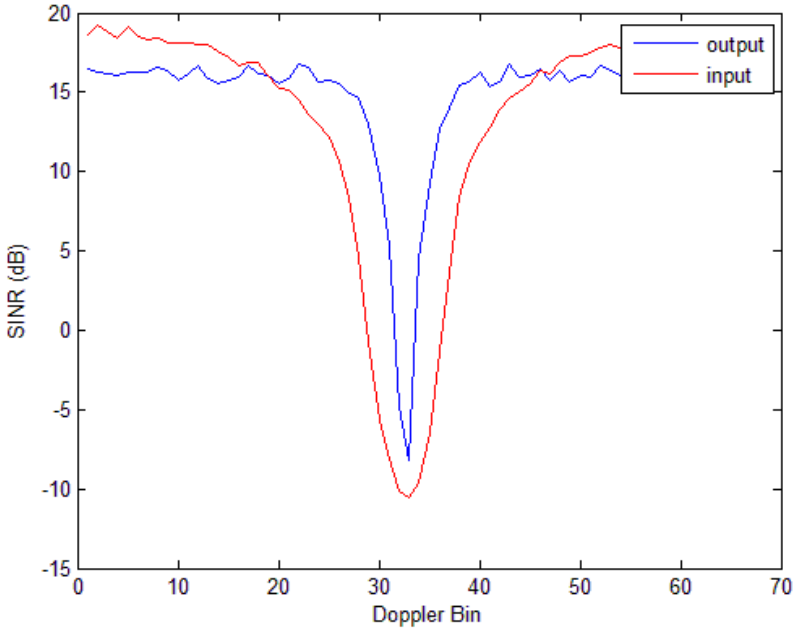


Figure 5.41: SMI Pre-Doppler STAP SINR Analysis for Clutter Simulation based on Flat Area SAR Image with K=40

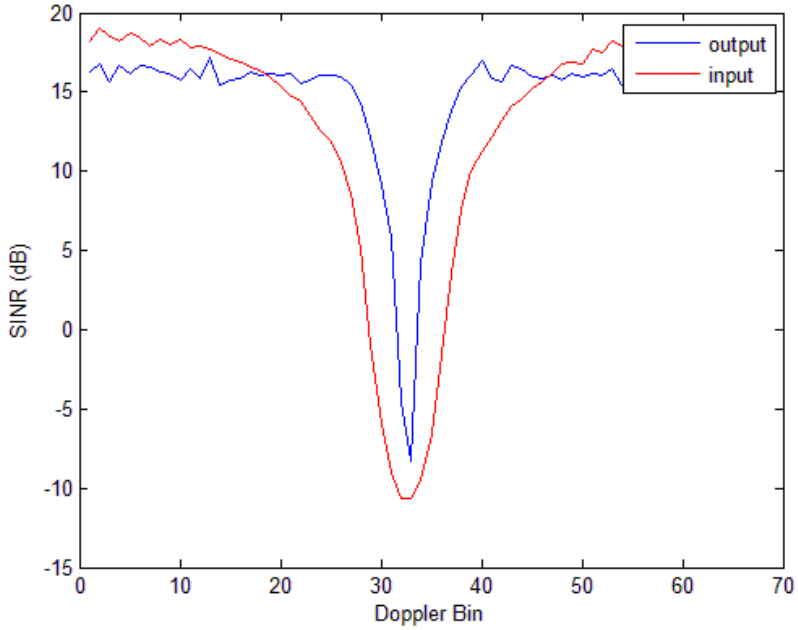


Figure 5.42: SMI Pre-Doppler STAP SINR Analysis for Clutter Simulation based on Hilly Area SAR Image with K=40

resulting detections and false alarms are observed. A sample output for SMI Pre-Doppler STAP filtering detection test statistics is shown in figure 5.43. CFAR output of the detection test statistics is illustrated in figure 5.44. In figures 5.43 and 5.44, range-Doppler bin corresponding to controlled moving target is marked with a yellow circle.

Flight test data results for SINR analysis of SMI Pre-Doppler STAP using 10 secondary range lines can be observed in Figure 5.45 for each CPI. Estimated mean SINR for $K = 10$ secondary range lines, is 9.5 dB. SINR values are estimated using neighbor range bins that have the same Doppler as the target. Similarly, flight test data results for SINR analysis of SMI Pre-Doppler STAP using 40 secondary range lines are illustrated in Figure 5.45 for each CPI. Estimated mean SINR for $K = 40$ secondary range lines, is 21 dB. Results for $K = 10$ secondary data are shown with blue line while results for $K = 40$ secondary data are shown with red line. Estimated target SINR results indicate that with smaller secondary sample support, SINR output of the SMI Pre-Doppler STAP filtering decreases dramatically.

Figure 5.46 illustrates the CFAR output of the detection test statistics obtained by SMI Pre-Doppler STAP filtering with $K = 10$ secondary range lines. Similarly Figure 5.47 illustrates the CFAR output of the detection test statistics obtained by SMI Pre-Doppler STAP filtering with $K = 40$ secondary range lines. For each CPI, detections obtained are marked with small circles on the range-Doppler map according to the range bin and Doppler bin of the detections. Detections for the controlled moving target are marked with a black circle. Cell averaging CFAR is performed for a false alarm probability of $10^{-6}$. Since the analysis is performed for 64 CPI, 128 Doppler bins, 96 remaining range bins and false alarm probability of $10^{-6}$, the expected number of false alarms is in the order of 1. Investigating the results shown in figure 5.47 and 5.46, it can be stated that with increasing secondary range lines ($K = 40$ ), number of detections of the controlled endoclutter target are higher than the small secondary sample case.

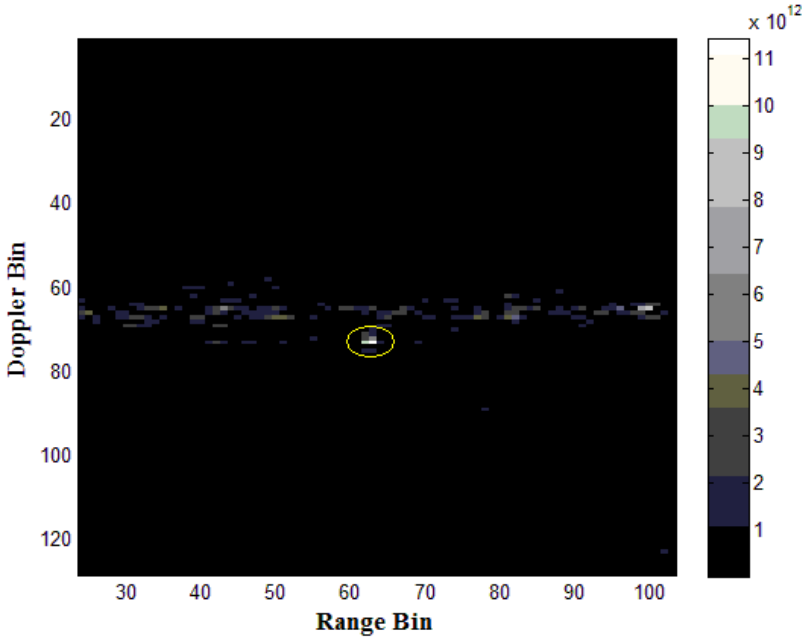


Figure 5.43: SMI Pre-Doppler Flight Test Data STAP Sample Detection Test Statistics (The target is the dot enclosed by the circle.)

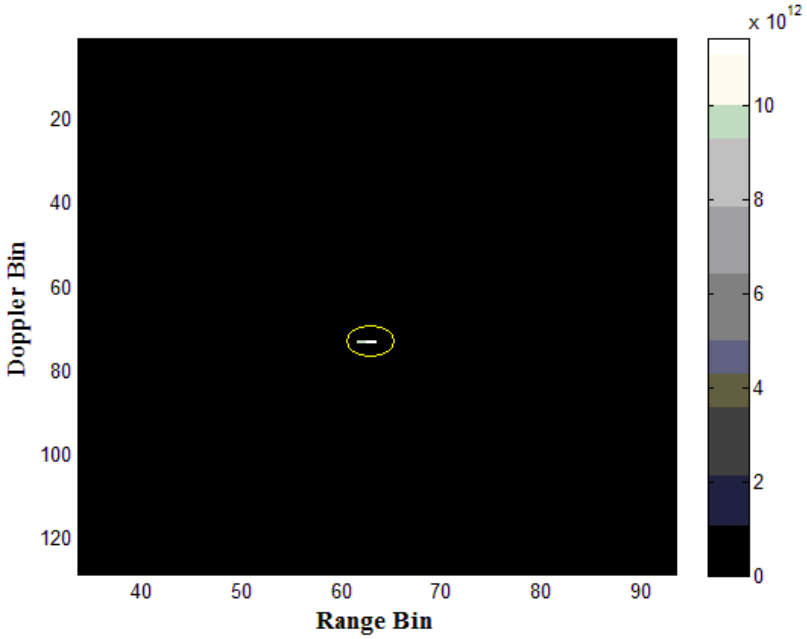


Figure 5.44: SMI Pre-Doppler STAP Flight Test Data Sample Detection Test Statistics CFAR Output (The target is the dot enclosed by the circle.)

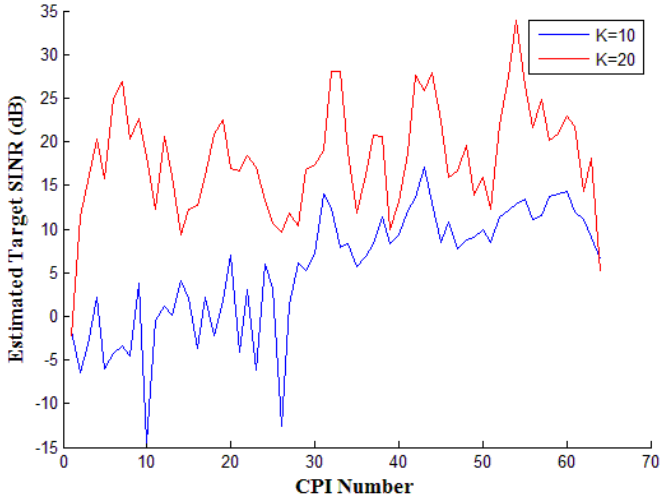


Figure 5.45: SMI Pre-Doppler STAP Flight Test Data SINR Analysis

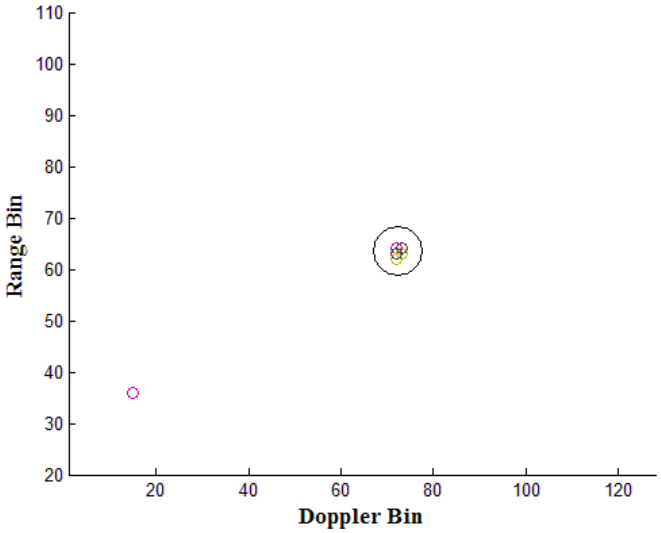


Figure 5.46: SMI Pre-Doppler STAP Flight Test Data Detection Test Statistics CFAR Detections for $K = 10$ (Detections due to the target are enclosed by the circle.)

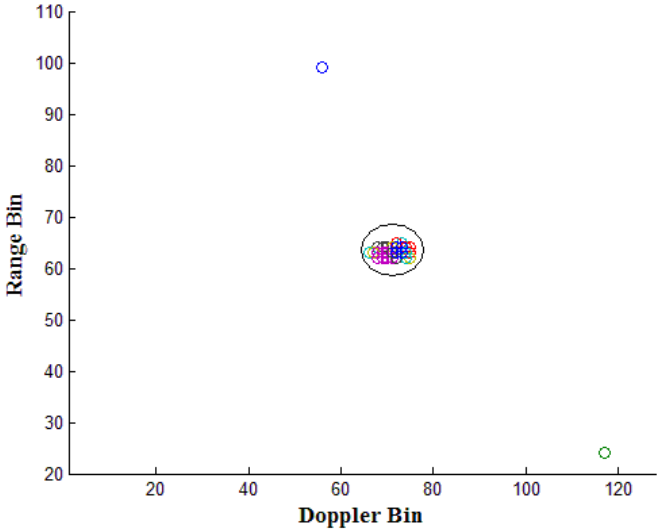


Figure 5.47: SMI Pre-Doppler STAP Flight Test Data Detection Test Statistics CFAR Detections for $K = 40$ (Detections due to the target are enclosed by the circle.)

# CHAPTER 6

# CONCLUSIONS

## 6.1 Thesis Summary

The main objective of this thesis was investigating the performance of parametric model based GMTI and space time autoregressive filtering. A GMTI simulator was developed to compare these clutter suppression techniques under various clutter distributions. Data acquired during flight tests with experimental SAR system were also used for evaluation of these approaches.

A basic theoretical review of GMTI geometry, Doppler structure for airborne radars, minimum detectable velocity concept, optimum and match filter detectors, sample matrix inversion (SMI) pre-Doppler STAP and parametric adaptive matched filtering were summarized.

Space time auto-regressive filtering was described by assuming a certain model for interference. STAR filter coefficient determination and STAR interference model order estimation were explained. Theoretical basis of STAR filtering was completed by describing the STAR weighting vector and computational requirement for vector element calculation.

A clutter covariance model was described for model based GMTI as well as the space time target steering vector model. For the clutter covariance model, clutter power estimation is required. For enhanced clutter power estimation, inner product non-homogeneity detector and the intelligent power estimation techniques are reviewed. Model-based GMTI theoretical basis was concluded with weighting vector calculation scheme and computational requirement for vector element calculation.

Performance of STAR filtering and model based GMTI were investigated using simulated data and flight test data. SMI pre-Doppler STAP was also implemented for comparison purposes. During the simulations statistical data, that has the required covariance for different clutter distributions, were generated. Clutter map based simulated clutter generation is performed as well as Gaussian and K-distributed clutter generation.

STAR filtering simulation results indicate that STAR filtering can tolerate usage of smaller number of secondary data with some graceful performance degradation unlike SMI pre-Doppler STAP which is unable to detect moving targets with small radial velocity in the case of small secondary data set. Despite the fact that STAR filtering performs well, under different clutter distributions for relatively high secondary sample support, when the secondary sample support is reduced, MDV performance degrades for K-distributed and hilly area SAR image based clutter since inhomogeneities and the clutter rank increases. Flight test results showed that with smaller numbers of secondary data, prediction error detection test statistics becomes spiky and loses its constant false alarm property under cell averaging CFAR. STAR filter model order selection was analyzed for AIC and MDL criterion. These criterion converges to similar model order numbers for both simulation data and flight test data. However MDL proved to be converging more rapidly than the AIC criteria. As a result, STAR filtering can be described as a structure-based parametric adaptive method which requires smaller secondary data sets for detection despite the increased false alarm rate.

Clutter power estimation approaches for model based GMTI are tested with simulation data. The intelligent power estimation method outperforms IP-NHD method while both estimation techniques perform similarly in case of target presence in the secondary data used for clutter power estimation. Model based GMTI was implemented by using the intelligent power estimation for simulation and flight test data. Simulation results indicates that the model based GMTI performs well under Gaussian clutter and flat areas. However, for the hilly area SAR image based clutter generation and K-Distributed clutter generation, larger MDV values are observed due to the inhomogeneities in the iso-range lines. Flight test data results illustrated the ability to detect endoclutter targets using interference covariance matrix model for clutter suppression. Estimated target SINR results for flight test data indicate that model based GMTI suffers additional SINR loss which may be a result of internal clutter motion, modeling imperfections and model assumption violations like platform velocity variation. Model-based GMTI can be described as a method that requires less computation capacity in return of some detection performance loss as a result of the factors that are not modeled such as internal clutter motion .

## 6.2 Future Work

There are some research possibilities that could not be performed within the scope of this thesis. Some of the topics that would require further investigation are:

- Usage of digital terrain elevation data (DTED) in the clutter covariance matrix model construction.
- Inclusion of internal clutter motion in the autocovariance model.
- Usage of Synthetic Aperture Radar images in the clutter covariance matrix model construction.
- Effects of a target in the secondary sample support on the STAR filtering.

# REFERENCES


[1] Brennan, L.E., Reed, I.S.: "Theory of adaptive radar", IEEE Trans. Aerosp. Electron. Syst., 1973, 9, (2), pp. 237–252

[2] Ward, J.: "Space-time adaptive processing for airborne radar". Technical report ESC 1015, MIT Lincoln Laboratory, Lexington, MA, 1994

[3] Guerci, J.R.: "Space-time adaptive processing for radar" (Artech House, 2003)

[4] Reed, I.S., Mallet, J.D., Brennan, L.E.: "Rapid convergence rate in adaptive arrays", IEEE Trans. Aerosp. Electron. Syst., 1974, 10, (6), pp. 853–863

[5] Carlson, B.D.: "Covariance matrix estimation errors and diagonal loading in adaptive arrays", IEEE Trans. Aerosp. Electron. Syst., 1988, 24, (4), pp. 397–401

[6] Kirsteins, I., Tufts, D.: "Adaptive detection using a low rank approximation to a data matrix", IEEE Trans. Aerosp. Electron. Syst., 1994, 30, (1), pp. 55–67

[7] Guerci, J.R.: "Space-time adaptive processing for radar" (Artech House, 2003)

[8] Roman, J.R., Rangaswamy, M., Davis, D.W., Zhang, Q., Himed, B., Michels, J.H.: "Parametric adaptive matched filter for airborne radar applications", IEEE Trans. Aerosp. Electron. Syst., 2000, 36, (2), pp. 677–692

[9] Y. Dong: "A modified parametric adaptive matched filter without dimensionality loss", International Conference on Radar, October 2006

[10] J. A. Russ, D.W. Casbeer, A. L. Swindlehurst,"STAP Detection Using Space-Time Autoregressive Filtering ", IEEE National Radar Conference Proceedings, May 2004.

[11] P. Parker and A. Swindlehurst, "Space-Time Autoregressive Filtering for Matched Subspace STAP ", IEEE Trans. on Aero. and Elec. Sys., vol. AES-39, no. 2, pp. 510-520, April 2003.

[12] Rissanen, J, "Modeling by shortest data description", Automatica, 14 (1978), 1978, pp.465-471.

[13] Akaike, H.: "A new look at the statistical model identification", IEEE Trans. Autom. Control, 1974, 19, pp. 716–723

[14] Melvin, W.L., Wicks M.C.: "Improving Practical Space-Time Adaptive Radar", IEEE National Radar Conference, 1997, pp. 48-53

[15] Smith, M.E., Varshney, P.K.:"Intelligent CFAR processor based on data variability", IEEE Transactions on Aerospace and Electronic Systems, Volume: 36, Issue: 3, Part:1, 2000, pp. 837-847

[16] P. Chen, "On testing the equality of covariance matrices under singularity," Report for AFOSR Summer Faculty Research Program, Rome Laboratory, Rome, NY, August 1994.

[17] C.Baktır, "Simulation-based Comparison of Some GMTI Techniques", METU EEE Master of Science Thesis, 2009

[18] G.Yıldırım, "Antenna Patterns for Detecting Slowly Moving Targets in Two Channel GMTI Processing", METU EEE Master of Science Thesis, 2010

[19] O.Eryiğit,“Interference Suppression by Using Space Time Adaptive Processing for Adaptive Radar”, METU EEE Master of Science Thesis, 2008

[20] E.Anadol, “A Knowledge Based Approach in GMTI for The Estimation of the Clutter Covariance Matrix in Space Time Adaptive Processing”, METU EEE Master of Science Thesis, 2012

[21] J.A.Richards, “GMTI Radar Minimum Detectable Velocity, Technical Report SAND2011-1767 ”, Sandia National Laboratories, Albuquerque, NM, April 2011

[22] Robey, F C, Fuhrmann, D R, Kelly, E J, and Nitzberg R, “A CFAR adaptive matched filter detector”, IEEE Trans on Aerospace and Electronic Systems, vol. 28, no. 1, pp. 208-216, 1992.

[23] Brennan, L., and Staudaher, E, “Subclutter visibility demonstration”, Technical reports RL-TR-92-2 1, Adaptive Sensors, Inc., 1992.

[24] M. Zatnian, “Circular array STAP”, IEEE Trans. on Aem. and Elec. Sys., vol. AES-36, pp. 510-517, Apr. 2000.

[25] Y.Tanık, “Private Report”, METU, 2009